Cell Reports

Article

# Body-fat sensor triggers ribosome maturation in the steroidogenic gland to initiate sexual maturation in *Drosophila*

## Graphical abstract

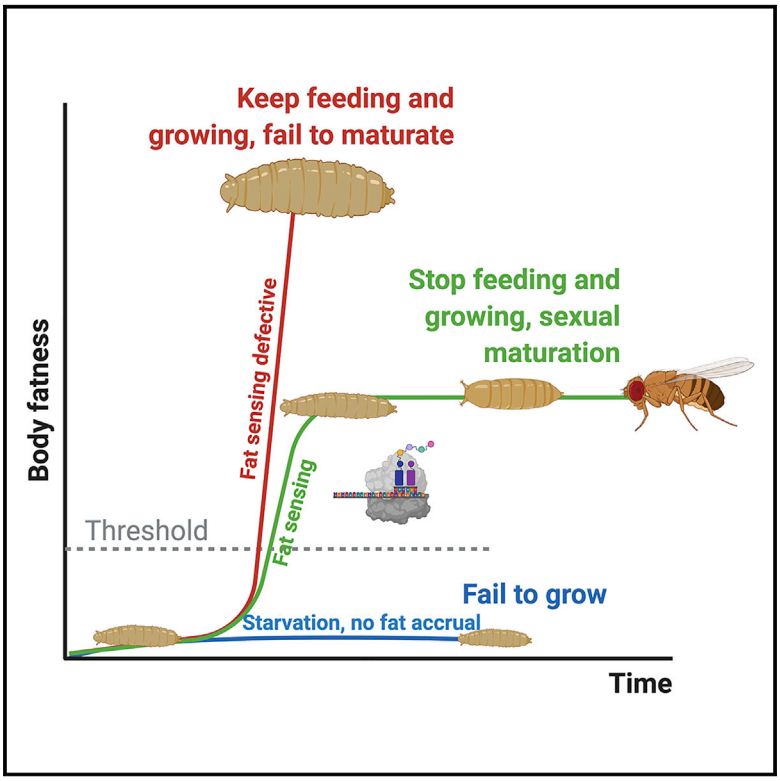


## Highlights

- An RNAi screen identifies body-fat signaling and sensing genes for maturation decision
- Lack of body-fat sensor mechanisms leads to giant, obese, and non-pupating larvae
- Semaphorin 1a triggers lipid/Apolpp-dependent trafficking and ribosome maturation
- Downstream, leptin-like upd2 signals feeding cessation and wandering transition

## Authors

Sergio Juarez-Carreño, Diana Marcela Vallejo, Juan Carranza-Valencia, ..., Antonio Pineda-Lucena, Maria Dominguez, Javier Morante

## Correspondence

m.dominguez@umh.es (M.D.), j.morante@umh.es (J.M.)

## In brief

Juveniles monitor peripheral fat for maturation commitment. Juarez-Carreño et al. identify a fat-cell-derived apolipophorin signaling that triggers prothoracic gland and organism maturation via a semaphorin 1a-mediated upd2/leptin.

Juarez-Carreño et al., 2021, Cell Reports *37*, 109830
October 12, 2021 
https://doi.org/10.1016/j.celrep.2021.109830

CellPress

Cell Reports

CellPress
OPEN ACCESS

Article

# Body-fat sensor triggers ribosome maturation in the steroidogenic gland to initiate sexual maturation in *Drosophila*

Sergio Juarez-Carreño,[1] Diana Marcela Vallejo,[1] Juan Carranza-Valencia,[1] Martina Palomino-Schätzlein,[2] Pol Ramon-Cañellas,[1] Roberto Santoro,[1] Emily de Hartog,[1,5] Dolors Ferres-Marco,[1] Aitana Romero,[1] Hannah Payette Peterson,[1] Esther Ballesta-Illan,[1] Antonio Pineda-Lucena,[3,4] Maria Dominguez,[1,*] and Javier Morante[1,6,*]

[1]Instituto de Neurociencias, Consejo Superior de Investigaciones Cientificas (CSIC), and Universidad Miguel Hernández (UMH), Campus de Sant Joan, Apartado 18, 03550 Sant Joan, Alicante, Spain

[2]Centro de Investigación Príncipe Felipe, Calle Eduardo Primo Yúfera, 3, 46012 Valencia, Spain

[3]Instituto de Investigación Sanitaria La Fe, Hospital Universitario y Politécnico La Fe, Avenida Fernando Abril Martorell, 106, 46026 Valencia, Spain

[4]Programa de Terapias Moleculares, Centro de Investigación Médica Aplicada, Universidad de Navarra, Avenida Pío XII, 55, 31008 Pamplona, Spain

[5]Present address: Groningen Institute for Evolutionary Life Sciences, University of Groningen, Nijenborgh 7, 9747AG Groningen, the Netherlands

[6]Lead contact

*Correspondence: m.dominguez@umh.es (M.D.), j.morante@umh.es (J.M.)

https://doi.org/10.1016/j.celrep.2021.109830

## SUMMARY

Fat stores are critical for reproductive success and may govern maturation initiation. Here, we report that signaling and sensing fat sufficiency for sexual maturation commitment requires the lipid carrier apolipophorin in fat cells and Sema1a in the neuroendocrine prothoracic gland (PG). Larvae lacking *apolpp* or *Sema1a* fail to initiate maturation despite accruing sufficient fat stores, and they continue gaining weight until death. Mechanistically, sensing peripheral body-fat levels via the apolipophorin/Sema1a axis regulates endocytosis, endoplasmic reticulum remodeling, and ribosomal maturation for the acquisition of the PG cells' high biosynthetic and secretory capacity. Downstream of apolipophorin/Sema1a, leptin-like upd2 triggers the cessation of feeding and initiates sexual maturation. Human Leptin in the insect PG substitutes for upd2, preventing obesity and triggering maturation downstream of Sema1a. These data show how peripheral fat levels regulate the control of the maturation decision-making process via remodeling of endomembranes and ribosomal biogenesis in gland cells.

## INTRODUCTION

The initiation of sexual development is correlated with profound changes in hormonal secretory activities of the pituitary gland in vertebrates and the steroidogenic prothoracic gland (PG) in insects. The actual trigger of sexual maturation is still undefined, but a pervasive factor controlling this transition is nutrition, or the mechanism that is coupled with attaining a critical or minimal body size, weight, or fatness (Kaplowitz, 2008). In rodents, the initiation of sexual maturation is linked to the body's energy state and growth (Baker, 1985; Kennedy and Mitra, 1963). In humans, puberty is delayed by anorexia nervosa (Katz and Vollenhoven, 2000) and intensive physical training (Frisch and Revelle, 1970) and is accelerated in overweight and obese children (Ahmed et al., 2009). These observations support the hypothesis that a body-fat "checkpoint" ensures that growing juveniles do not commit to reproductive maturation unless they have adequate energy stores to meet the demands of reproduction (critical fatness hypothesis) (Kaplowitz, 2008). The association is supported by observations in humans and mice deficient for the hormone leptin, which is made by fat cells, signals satiety, and is also required for sexual maturation (Clément et al., 1998; Friedman and Halaas, 1998; Montague et al., 1997), because such a deficiency of leptin or its receptor delays puberty or completely fails its initiation, accompanied by hyperphagia and progressive obesity.

In insects, the commitment to metamorphosis and sexual maturation is unequivocally dependent on nutrition. Growing larvae must attain a certain "critical weight" (CW; Nijhout and Williams, 1974) before metamorphosis is possible. Once larvae surpass it, a still ill-defined process is set in motion that leads to a small release of the steroid prohormone ecdysone from the PG (the "commitment" pulse; Berreur et al., 1979) and culminates about 2 days later with another surge of ecdysone, believed to be the trigger to cease feeding, initiate wandering, and enter into the pupal stage (Yamanaka et al., 2013) (Figure 1A). No morphological correlates with the CW point have yet been identified.

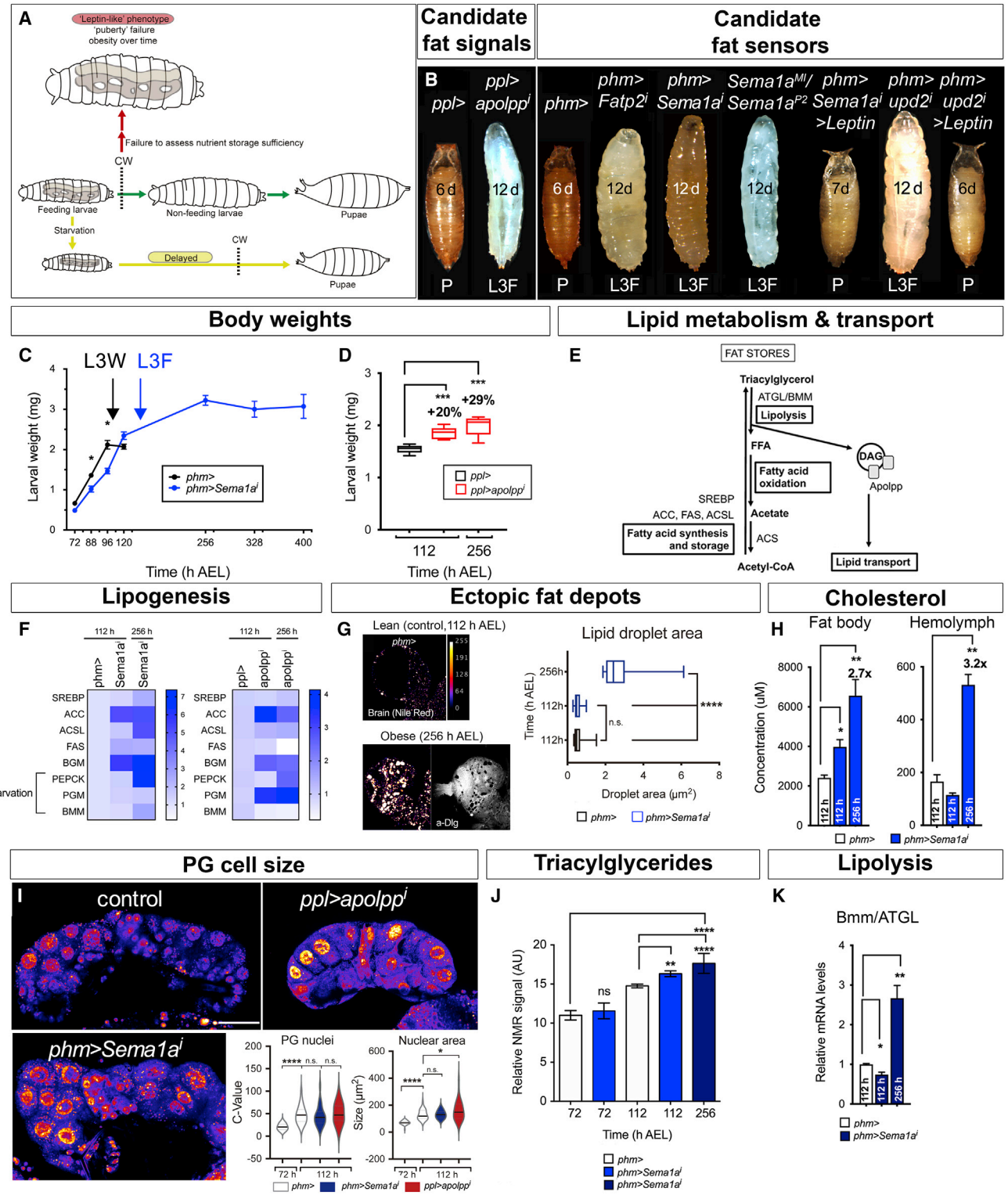


**Figure 1. Identification of candidate factors for the critical weight (CW)-sensing mechanism for maturation commitment**

(A) Diagram representing feeding larvae and fat body as they become irreversible committed to maturation after exceeding the CW. Post-CW larva continues to grow and feed for another 24–36 h, then stops feeding and starts pupal formation. Starving before CW prevents the attainment of sufficient fat for this pupal commitment. It is hypothesized that failure to sense energy reserves would keep larvae in pre-CW, resulting in juvenile obesity phenotype similar to that of *Leptin* mutants.

*(legend continued on next page)*

The PG grows progressively during the last larval stage (third instar in *Drosophila melanogaster*) (Caldwell et al., 2005; Mirth et al., 2005) through a nutrient-dependent endoreplication process that is mediated by the conserved insulin/phosphoinositide 3-kinase (PI3K) and target of rapamycin (TOR) pathways (Koyama et al., 2014; Ohhara et al., 2017). Larval starvation, or genetic manipulation of insulin/PI3K and TOR signaling in the PG, impairs gland size and overall larval growth, preventing or delaying the acquisition of the threshold of weight for the onset of metamorphosis (Caldwell et al., 2005; Colombani et al., 2005; Mirth et al., 2005). This insulin/TOR control temporally coincides with the CW point, meaning the CW is indistinctly referred to as a critical size or weight checkpoint. Body weight largely correlates with fat content (Church and Robertson, 1966a), but little is known about how body fat is signaled and sensed in insects for the commitment to maturation.

Macropinocytosis is an evolutionarily conserved endocytic mechanism normally involved in the uptake of fluids, nutrients, and macromolecules (Palm and Thompson, 2017). It is also used for the uptake of steroid hormone precursors by PG cells during the feeding period (Blazsek and Mala, 1978). Macropinocytosis can occur spontaneously or be a regulated process often involving Rab family proteins (Bloomfield and Kay, 2016; Swanson, 2008). The release of synthesized steroid hormones then occurs by a reverse process involving exocytosis and vesicle trafficking (Cruz et al., 2020; Yamanaka et al., 2015). The uptake and release processes are not simultaneous, but the signals that time the order of these processes are not known.

To link biosynthesis with secretion for triggering sexual maturation, mechanisms controlling transcription, translation, and secretion need to be coupled in a switch-like manner. It has been shown recently that the ecdysone surges from the PG after the CW point are coincidental with synchronous and global changes in gene expression dynamics (Andres et al., 1993; Graveley et al., 2011; Lockett and Ashburner, 1989), including changes in ribosomal genes. Ribosomes are the essential machinery for protein synthesis, and ultrastructural analysis of third instar PGs before and during high secretory activity has shown that ER membranes undergo major remodeling and enrichment in ribosomes via unknown mechanisms (Aggarwal and King, 1969; Dai and Gilbert, 1991). Ribosome biogenesis is regulated by starvation, but the essential nutrient cues and signaling pathways mediating nutritional control of translation in *D. melanogaster* larvae remain incompletely understood (Nagarajan and Grewal, 2014). Enhanced ribosome biogenesis is positively correlated with maturation in some insects (Wang et al., 2017), and inactivation of a ribosomal protein, *RpS6*, delays metamorphosis and reduces ecdysone synthesis (Lin et al., 2011). However, despite the importance of insulin/PI3K/TOR in protein synthesis and PG cell growth (Mirth and Riddiford, 2007), activation of the canonical effector of TOR signaling the ribosome regulator S6 kinase cannot rescue the loss of insulin/TOR activity in the PG (Koyama et al., 2014; Ohhara et al., 2017). Another regulator of ribosome biogenesis and protein synthesis is Myc; it is also not necessary for the PG-related maturation process (Li et al., 2010). Thus, the gene(s) involved in ribosome biogenesis and maturation during CW remains unknown.

To investigate how critical body weight is signaled and sensed for maturation commitment in *D. melanogaster*, we used RNA interference (RNAi; *RNA$^i$*)-based screens to identify (1) genes encoding nutrient transporters and (2) secreted and transmembrane proteins whose silencing resulted in a failure to initiate sexual maturation despite sufficient body weight being attained.

## RESULTS

### Lipid transporter genes link adiposity to maturation initiation

The mechanisms that represent overall body weight or energetic status, endocrine or otherwise, are not yet defined in insects. This is, in part, because loss of leptin-like hormone *upd2* in the fat body (equivalent to adipose tissue in vertebrates) does not phenocopy the expected obesity and failure of puberty seen in *Leptin* mutations in rodents and humans (Clément et al., 1998; Friedman and Halaas, 1998; Rajan and Perrimon, 2012).

To identify what macronutrient(s) may be sensed by the PG for pupal commitment, we used *RNA$^i$* to systematically knock down nutrient transporter genes for lipids, amino acids, and carbohydrates (Musselman et al., 2011) in the PG using *phantom* (*phm*)-*Gal4*.

Silencing (seven independent *slif RNA$^i$* lines tested) the cationic amino acid transporter *slimfast* (*slif*), which is proposed to act in amino acid sensing and TOR activation in the fat body, did not prevent larval-pupal transition (Figure S1A). Lines were verified to produce the expected effect in the fat body

(B) Shown are *RNA$^i$* knockdown of *apolpp*, *Fatp2*, *Sema1a*, and *upd2* in the fat body (*ppl > apolpp$^i$*) or in the PG (*phm > Sema1a$^i$*; *phm > Fatp2$^i$* and *phm > upd2$^i$* are shown in Figure 7) or endogenous mutations of *Sema1a*. Shown are representative animals at 12 days AEL and control pupae (*ppl>* and *phm>*). PG-specific human Leptin expression in *phm > Sema1a$^i$* and *phm > upd2$^i$* larvae.
(C) Time course of larval weight in control *phm>* (black line) and *Sema1a$^i$* (blue line).
(D) Larval weight of control *ppl>* and *apolpp$^i$*.
(E) Schematic of tested enzymes participating in fatty acid synthesis, storage, and oxidation.
(F) Heatmap of qRT-PCR data in control, *Sema1a$^i$*, and *apolpp$^i$* mutants.
(G) Pseudocolored super-resolution images of larval brains of *phm>* at 112 h and *Sema1a$^i$* at 256 h AEL (left) and quantification of fat depots (right). Cell membranes (anti-Dlg) and neutral lipids (Nile Red).
(H) Cholesterol levels in the fat body and circulating hemolymph in the indicated genotypes and ages.
(I) Pseudocolored super-resolution images and quantifications of C values of PG nuclei (left) and nuclear size (right) of the indicated genotypes and ages.
(J) $^1$H-NMR signal for triacylglycerol levels over time (and Table S5).
(K) *Bmm/ATGL* in control and mutants.
Data are mean ± SEM. *p < 0.05, **p < 0.01, ***p < 0.001, ****p < 0.0001, unpaired t test except two-way ANOVA in (F). In all panels, representative larvae or pupae (n = 20–30) of genotypes and age are shown. L3F, feeding third instar larvae; L3W, wandering larvae; P, pupae.

(Figure S1A; Table S1). Silencing other cationic amino acid transporters (*CG5535*, *CG7255*, *CG12531*, *G13248*, and *tadr*) also had no effect (Table S1). Silencing sugar transporters (*Glut1* and *Glut3*, *sut1-sut4*, *Tret1-1*, and *Tret1-2*) also did not prevent the larval-pupal transition (Table S1). This suggested that the PG may sense other nutrient types.

Indeed, silencing the member of the SLC27 family of fatty acid sensing, *Fatty acid transporter protein 2* (*Fatp2*), which is a key transporter of long-chain fatty acids, in the PG resulted in larvae that never left the food and continued growing and gaining weight until death (Figure 1B) analogously to the effects of *Leptin/LepR* loss in patients and mice.

These data hint at a fat-sensor mechanism in the larval PG coordinating body weight and growth for pupal commitment.

## RNAi-based screen for genes signaling and sensing adiposity to maturation initiation

Inspired by *Leptin/LepR* mutants (Figure 1A), we devised an unbiased *RNA$^i$*-based screen to identify genes that, when silenced, produce animals unable to monitor adiposity for commitment to metamorphosis despite reaching sufficient body weight (Figure S1B). To identify candidate adiposity signaling/sensing, we screened a random set of genes encoding secreted and transmembrane proteins (Table S2).

*mir-8-Gal4* was selected to drive RNA$^i$ lines simultaneously in the fat body [equivalent to mammalian adipose tissue and liver (Arrese and Soulages, 2010)], PG (Figures S1B–S1D), and cortex glia (Morante et al., 2013). Hits were retested in a secondary screen for fat-body-specific knockdown using *pumpless* (*ppl*)-*Gal4* (Zinke et al., 1999), and *phm-Gal4* (Ono et al., 2006) and *spookier* (*spok*)-*Gal4* (Moeller et al., 2017) for PG-specific knockdown (see Figures 1B, S1B, and S1E).

In this way, we selected the lipid carrier apolipophorin (*apolpp*), the axon guidance protein Semaphorin1a (*Sema1a*), and TGF-$\alpha$ *spitz* (*spi*) as candidate genes for adiposity signaling and CW sensing for metamorphosis commitment (Table S2). *spi* was identified recently as a regulator of ecdysone (Cruz et al., 2020). We validated Sema1a using endogenous mutations *Sema1a$^{MI00031\text{-}GFSTF.2}$* (Nagarkar-Jaiswal et al., 2015) and *Sema1a$^{P2}$* (Yu et al., 1998) in pupal commitment (Figure 1B).

Remarkably, the functional analog of human *Leptin* (Rajan and Perrimon, 2012), *upd2*, was also identified (Figures 1A and S1F and see below). Validating our screen design, human *Leptin* expressed in the PG rescued both the non-pupating and obesity phenotype of *upd2$^i$* and *Sema1a$^i$* (Figure 1B).

## Non-pupating with massively obese phenotype

Apolpp, a member of the ApoB family (also known as lipophorin, lpp, Rfabp, or Rfabg) (Kutty et al., 1996), is the protein moiety of lipophorin and the main lipid carrier in insects (Palm et al., 2012). Lipophorin particles complexed with apolpp protein carry the bulk of hemolymph lipids and sterols and are exclusively produced by fat-body cells in proportion to fat content (Arrese et al., 2001; Palm et al., 2012). Thus, apolpp is a strong candidate to mediate adiposity information.

Knockdown of *apolpp* via *mir-8-Gal4* results in small larvae (Figure S1E), equivalent to the effects of starvation. However, a weaker knockdown via *ppl-Gal4* allowed (*ppl* > *apolpp$^i$*, hereafter *apolpp$^i$*) larvae to gain weight but failed to undergo metamorphosis (Figure 1B; see comments in Figure S1E). Four independent RNA$^i$ lines were tested. PG-specific silencing of *apolpp* did not affect metamorphosis or weight (Figure S1E). Thus, fat-body-derived lipids, lipophilic molecules, or apolpp itself is crucial for the maturation commitment decision process in *Drosophila*.

Sema1a is a repulsive axon guidance (Yu et al., 1998), and its silencing in the PG uncovered its central role for sexual maturation commitment acting in the PG (Figures 1B, S1E, and S1F). Mammalian semaphorins also regulate puberty onset through the control of the maturation neuroendocrine system (Känsäkoski et al., 2014). Intriguingly, Sema1a protein was shown physically to interact with apolpp in embryos (Rees et al., 2011), consistent with Sema1a and apolpp sharing a common non-pupating phenotype.

*Sema1a$^i$* phenotype is rescued by the expression of full-length (FL) *Sema1a* cDNA (Jeong et al., 2012) (Figures S1G and S1H, and see Figure S1I). Because membrane-bound semaphorins are capable of bidirectional signaling (Hernandez-Fleming et al., 2017; Jeong et al., 2012), serving as both ligand and receptor, we investigated whether Sema1a may act as a receptor or ligand in this process. Sema1a lacking the carboxy-terminal intracellular domain acted as a dominant-negative receptor (Jeong et al., 2012) phenocopying *Sema1a$^i$* and endogenous animals (*phm* > *Sema1a$^{ECD}$*; Figures S1H and S1J), consistent with Sema1a acting as a receptor. Neither the canonical Sema1a ligands, Sema2a and Sema2b, nor the canonical receptors, plexin A and B (Yazdani and Terman, 2006), phenocopy *phm* > *Sema1a$^i$* (hereafter *Sema1a$^i$*; Figure S1J; Table S3). Thus, the function of Sema1a in the PG is non-canonical.

## Obesity in non-pupating larvae is associated with signs of chronic starvation

We performed time-course analyses of weight gain (Figures 1C and 1D) and growth (Figures S1K and S1L) in *Sema1a$^i$* and *apolpp$^i$*. The body mass and size of these animals increased at a rate similar or slightly slower to that of control larvae. However, whereas the control larvae stopped feeding and growing at 120 h after egg laying (AEL) (Church and Robertson, 1966a), *Sema1a$^i$* and *apolpp$^i$* larvae continued growing until they reached a plateau (Figure 1C).

*Sema1a$^i$* larvae are opaque, suggesting excess fat accumulation (Woods et al., 1998). We measured the expression of genes participating in lipid homeostasis (Figure 1E) and global energy reserves and metabolites related to energy production using $^1$H nuclear magnetic resonance spectroscopy (NMR) (Tables S4 and S5). Compared with control larvae, *Sema1a$^i$* larvae showed higher expression of lipogenic-related genes, including sterol regulatory element binding protein (*SREBP*), acetyl-CoA carboxylase (*ACC*), long-chain fatty acyl-CoA synthetase (*Acsl*), acyl-CoA synthase bubblegum (*bgm*), and fatty acid synthase (*FAS*) (Figure 1F), as well as severe dyslipidemia (Figure 1G) and hypercholesteremia (Figure 1H). *Drosophila* is a cholesterol auxotroph (Hobson, 1935), and all transport of dietary cholesterol to tissues requires apolpp (Palm et al., 2012). Stores measured directly in fat bodies and circulating cholesterol were higher in the mutant than in control larvae. Judging by their

giant larval size, which places a great demand on lipid metabolism for membrane construction (Kunte et al., 2006), *Sema1a*$^{i}$ larvae probably have no deficits in the absorption of cholesterol and lipids. Remarkably, however, *Sema1a*$^{i}$ PG cells do not internalize fat-derived apolpp (see below). *Sema1a*$^{i}$ PGs are distinctly different from those with knockdown in the insulin/TOR pathways in that we did not detect any alteration in the size or endoreplication of the PG cells (Figure 1I and see below), which has been mechanistically linked to metamorphosis failure caused by insulin/TOR knockdown (Layalle et al., 2008; Ohhara et al., 2017).

Despite levels of triacylglycerol being significantly greater in the mutant as measured using $^{1}$H-NMR (Figure 1J; Table S5), obese *Sema1a*$^{i}$ larvae showed metabolic alterations seen in starved animals. For example, levels of adipose triglyceride lipase (*ATGL* or *PNPLA2*) brummer (*bmm*), a central lipase in breaking down fat depots into free fatty acids (Grönke et al., 2005), were significantly higher in 12-day-old *Sema1a*$^{i}$ larvae than in lean control larvae (Figure 1K).

In summary, despite gaining at least three times the weight needed for maturation, *Sema1a*$^{i}$ larvae failed to commit to metamorphosis. This massive fat storage is associated with starvation-like changes, supporting that lack of *Sema1a* in the PG makes larvae unable to sense body energy stores.

## Chronic food intake independent of insulin signaling

Obesity could be secondary to the arrest in pre-CW. Supporting this idea, *Sema1a*$^{i}$ and *upd2*$^{i}$ larvae never exited the food. Using colored food that is retained in the gut for only 1 h approximately, we confirmed that mutant larvae continued eating, even after reaching massive weight (Figure 2A), reminiscent of the chronic food-seeking behavior in *Leptin/LepR* mutants (Friedman and Halaas, 1998; Gueorguiev et al., 2001).

To further examine this chronic feeding, we measured carbohydrate metabolism and insulin signaling (Figure 2B). *Sema1a*$^{i}$ larvae that stayed in the third instar stage for 8–12 days had elevated hemolymph glucose levels (Figure 2C), 52% more than control larvae at 256 h, but continued feeding. Overall carbohydrate stores (glycogen; Figure S2A), circulating trehalose (Figure S2B), and free amino acids (Figures S2C and S2E) in *Sema1a*$^{i}$ mutant larvae were similar to or slightly higher than in control larvae (Tables S4 and S5).

Chronic feeding in the *Sema1a*$^{i}$ larvae, despite hyperglycemia, could reflect a glucose or insulin resistance syndrome. Glucose sensing and clearance is known to rely on hexokinase C (*Hex-C*), the homolog of the maturity-onset diabetes of the young (*MODY-2*) gene (Mattila and Hietakangas, 2017). Elevated *Hex-C* mRNA levels in *Sema1a*$^{i}$ larvae (Figure 2D) indicate normal glucose regulation. Compared with control animals, mutant larvae had significantly upregulated expression of phosphoglycerate mutase (*PGAM1*) and phosphoenolpyruvate carboxykinase 1 (*Pepck1*) enzymes (Figure 2D) and changes in metabolites, such as citrate (Figure S2D; Table S4), that participate in gluconeogenesis.

Although diet-induced obesity has been associated with insulin resistance (Musselman et al., 2011), obesity in *Sema1a*$^{i}$ animals occurred without measurable impairment in the insulin/insulin-like growth factor signaling (IIS) pathway (Figure 2E). Expression of the major insulin/IGF-like peptides (ILPs), *Ilp2*, *Ilp3*, and *Ilp5* (Figure 2E), which mediate systemic growth and metabolic regulation (Grönke et al., 2005), was normal or slightly lower in *Sema1a*$^{i}$ larvae at 112 h than in control larvae. *Ilp*3 was elevated in older *Sema1a*$^{i}$ larvae (Figure 2E). Measurement of ILP2 accumulation in insulin-producing cells did not detect abnormalities in *Sema1a*$^{i}$ animals (Figures 2F, 2G, and 2I). Retention of ILP2, albeit small, was observed in the *upd2*$^{i}$ condition (Figures 2H and 2I). However, this did not translate to measurable changes in IIS. This shows that defects cannot be attributed to abnormal ILP2 secretion or signaling.

Activated insulin receptor (InR) inhibits the forkhead transcription factor FOXO (Eijkelenboom and Burgering, 2013). Because such expression levels of the FOXO target genes serve as a readout of the systemic IIS pathway, *InR*, *4E-BP/Thor*, and *Ilp6* were reduced in *Sema1a*$^{i}$ larvae (Figure 2E). Larvae *apolpp*$^{i}$ showed normal systemic IIS signaling (Figure 2E).

## Sema1a is essential for progression through the CW point

To further verify that Sema1a is required at the CW checkpoint (Figure 3A; Rewitz et al., 2013), we temporally control *Gal4/RNA*$^{i}$ using the thermosensitive *Gal80* repressor construct (*tub-Gal80*$^{ts}$; McGuire et al., 2003), which allows resolution analysis of gene activity in relation to the CW (e.g., Ohhara et al., 2017). Larvae with depleted *Sema1a* in the PG only after CW metamorphosed at identical time and weight as control (Figure 3B), demonstrating that Sema1a is specifically required for CW, and that obesity is a secondary consequence of failure to progress through the CW.

## Activation of nutrient-sensing insulin/TOR or PTTH/Ras pathways in the PG does not correct Sema1a defects

We next asked whether activation of insulin/TOR (Koyama et al., 2014; Ohhara et al., 2017; Yamanaka et al., 2013) (Figure S3A) and the PTTH/Torso/Ras (Caldwell et al., 2005; McBrayer et al., 2007; Rewitz et al., 2009) pathways, known to stimulate ecdysone biosynthesis, could bypass the Sema1a requirement (Figure 3C). Neither IIS/TOR nor *Ras*$^{V12}$ (or of the constitutively active Torso receptor (Rewitz et al., 2009) or of *S6K*, *S6K*$^{TE}$, and *Rheb*) corrected for the larval arrest and obesity caused by *Sema1a* depletion (Figures 3C and S3A; Table S3). This shows that Sema1a is an absolute requirement for progression through the CW commitment point.

## Giant arrested *Sema1a*$^{i}$ larvae progress toward metamorphosis when ecdysone is supplied exogenously

The attainment of CW is followed 24–36 h later by a rise in the expression of ecdysone biosynthetic genes *phm* and *disembodied* (*dib*), but *Sema1a*$^{i}$ larvae did not show this increase (Figures 3D and S3B) or the expected increase in the ecdysone target genes, *EcR* and *E75* (Figures 3D and S3B), which reflect failure in ecdysone production.

We attempted to rescue *Sema1a*$^{i}$ non-pupating and obesity defects by oral steroid prohormone supplementation. Feeding Sema1a$^{i}$ larvae at 72 h, either the prohormone α-ecdysone, which is normally converted into the active form 20-hydroxyecdysone (20E, formerly β-ecdysone) in peripheral tissues, or the

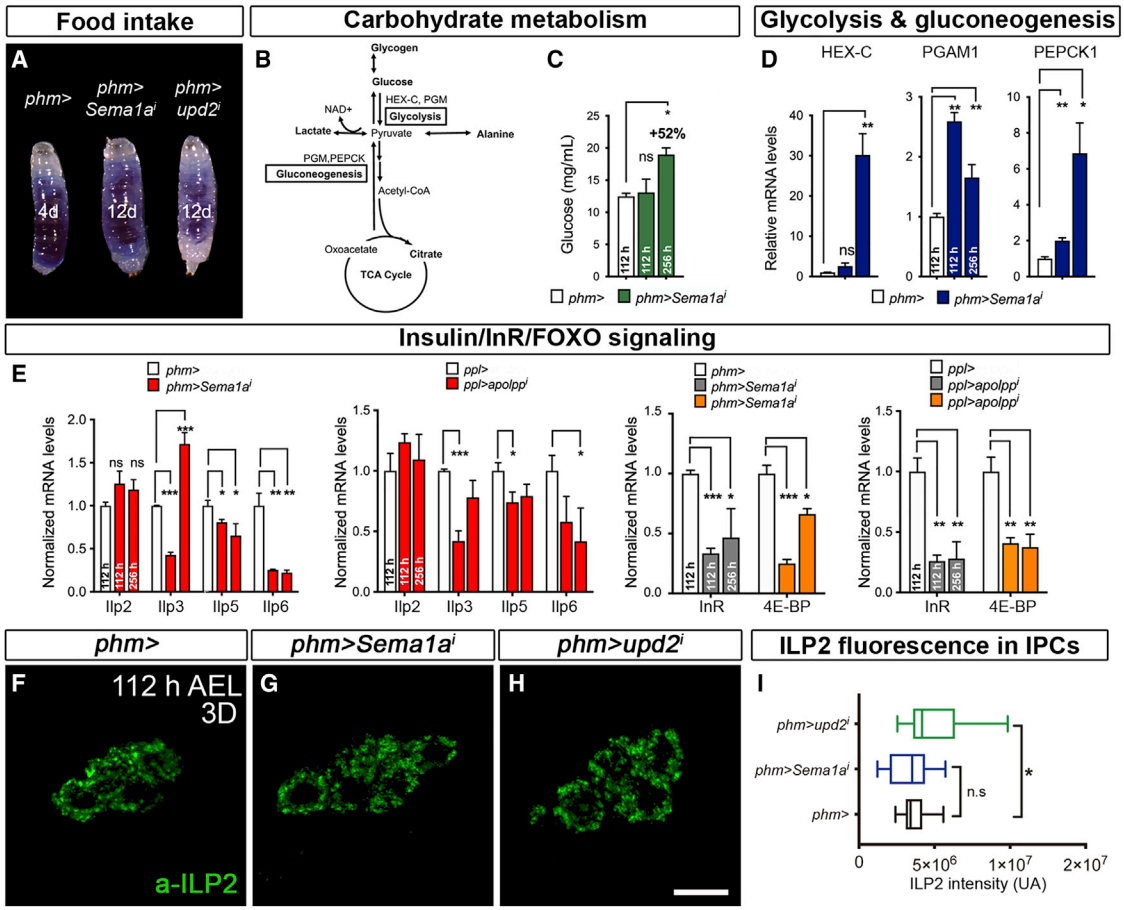


**Figure 2. Non-pupating, obese larvae show chronic feeding and starvation response**

(A) Food intake of control, *Sema1a*$^{i}$, and *upd2*$^{i}$ at the indicated ages.

(B) Schematic of examined enzymes involved in gluconeogenesis and glycolysis.

(C) Hemolymph glucose levels in control and *Sema1a*$^{i}$.

(D) qRT-PCR data of *Hex-C*, *PGAM1*, and *Pepck1*.

(E) qRT-PCR expression of insulin/FOXO signaling components.

(F–H) 3D reconstruction of super-resolution images of anti-ILP2 in brain neurosecretory cells (green).

(I) Quantification of ILP2 fluorescence intensities.

Data are mean ± SEM. *p < 0.05, **p < 0.01, ***p < 0.001, unpaired t test. Scale bar, 10 μm. ns, non-significant.

already active form 20E enabled all *Sema1a*$^{i}$ larvae to metamorphose (Figures 3E and S3C).

Remarkably, the giant *Sema1a*$^{i}$ larvae had small imaginal discs: the epithelial tissues that form the adult pharate (Figures S3E and S3F). The growth-stunted discs did not activate a size checkpoint mediated by the relaxin hormone Ilp8 (Garelli et al., 2012; Figure S3D), and neither could silencing *Ilp8* (*tubulin-α* > *Sema1a*$^{i}$ > *Ilp8*$^{i}$) correct the developmental arrest of Sema1a$^{i}$ larvae (Table S3). This indicates that Sema1a$^{i}$ larvae are arrested before this size checkpoint (Yamanaka et al., 2013). Growth-stunted imaginal disc in other giant, non-pupating mutants is linked to lack of ecdysone (Gibbens et al., 2011). Consistently, exogenous ecdysone administration re-activated this growth in 12-day-old giant Sema1a$^{i}$ larvae yielding to gigantic pharates (Figure 3E). In sum, although *Sema1a*$^{i}$ PG cells do not produce ecdysone, peripheral tissues can convert the prohormone into its active form and are competent to respond to 20E.

## Ontogenetic analysis of PG cell maturation using super-resolution imaging

Hence we performed a developmental time-course analysis of PG cell membranes in control and mutants using super-resolution imaging at two carefully staged time points: 72 h AEL, which in control larvae are at pre-CW, and 112 h (wandering stage in our culture conditions).

First, we verified that fat-body-derived apolpp reached and entered PG cells (Figures 4A and 4B and insets) (Igarashi et al., 2018; Kutty et al., 1996). We confirmed apolpp was of fat body origin because apolpp staining disappeared from PGs of larvae with knockdown of *apolpp* in the fat body (*ppl* > *apolpp*$^{i}$) (Figure 4D). Apolpp is retained in the plasma membrane of *Sema1a*$^{i}$ PGs (Figure 4C), and its expression is also regulated by the CW via Sema1a. Thus, although the attainment of CW was followed by a rise in the expression of *apolpp* in control larvae, levels remained low in *Sema1a*$^{i}$ mutants (Figure 4F). These observations

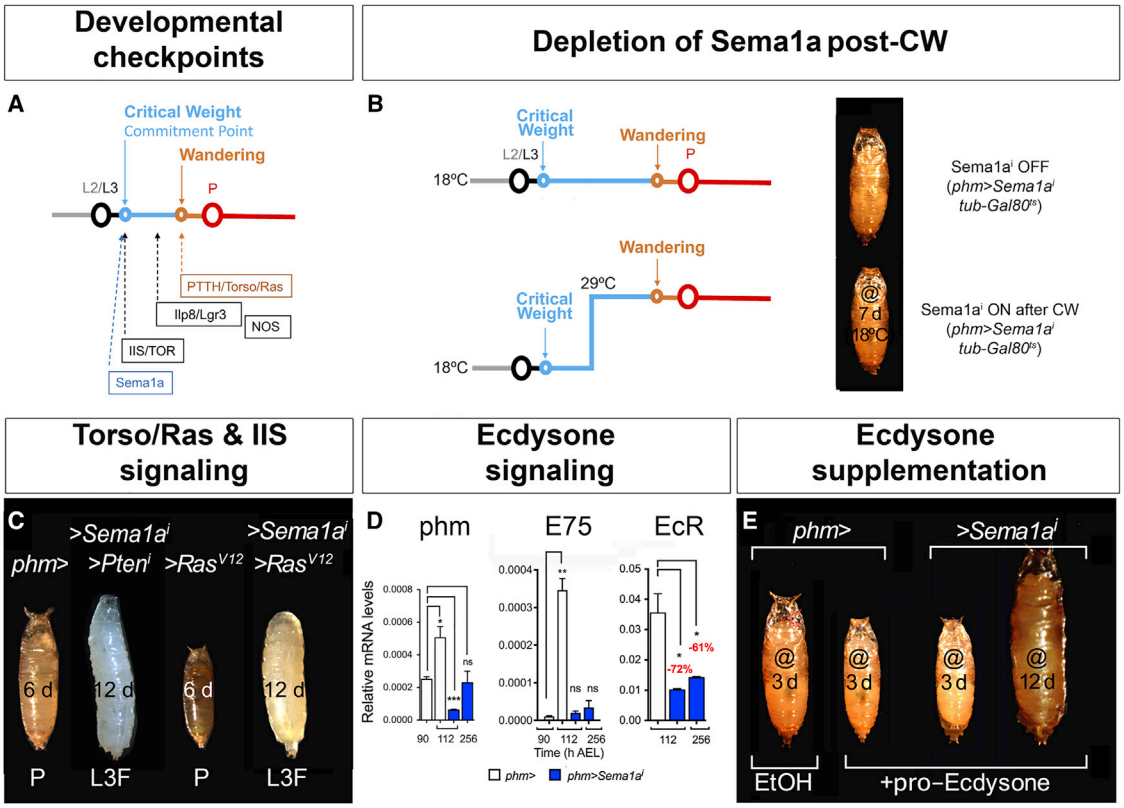


**Figure 3. Relationship of the CW checkpoint with other developmental checkpoints**

(A) Timeline of developmental checkpoints for the onset of metamorphosis.

(B) Depletion of *Sema1a* after CW does not prevent larval-pupal transition (*phm* > *Sema1a*$^{i}$; *tub-Gal80*$^{ts}$).

(C) Expression of *Pten*$^{i}$ or *Ras*$^{V12}$ in *phm* > *Sema1a*$^{i}$.

(D) *Phm*, *E75*, and *EcR* mRNA transcript levels analyzed by qRT-PCR.

(E) Pupa resulting after administration of pro-ecdysone (αE) at 72 h and at 256 h AEL.

Data are mean ± SEM. *p < 0.05, **p < 0.01, ***p < 0.001, unpaired t test. Representative larvae or pupae (n = 20) are shown.

show bidirectional communication between the fat body and the PG. Given that inhibiting lipid transport in the PG via *Fatp2* knockdown precludes the transition through the CW, we reasoned that lipids are at the core of the maturation commitment decision.

Mammalian semaphorins act in endocytosis and exocytosis, membrane remodeling, and trafficking (Alto and Terman, 2017). Macropinocytosis, a regulated endocytosis, is known to facilitate the uptake of large macromolecules, such as lipoprotein particles. Ultrastructural evidence indicates macropinocytosis-like events in early PGs (Aggarwal and King, 1969; Dai and Gilbert, 1991).

To functionally assess endocytosis in *Sema1a*$^{i}$, we blocked endocytosis via the small GTPase Rab5 (Kiral et al., 2018) and found it mimicked the effect of *Sema1a*$^{i}$ (Figures 4E and 4G). Importantly, enforced expression of *Rab5* fully rescued the *Sema1a*$^{i}$ defects (*phm* > *Sema1a*$^{i}$ > *Rab5*) (Figure 4G). Thus, endocytosis is a prerequisite for the CW downstream of Sema1a (Figure 4H).

We hypothesized that uptake of critical circulating signals, such as lipid/apolpp, provides the trigger for CW. To link this to ecdysone production and/or secretion, we examined when PG acquires its secretory capacity. We marked the plasma membrane using *mCD8::GFP*, which contains a KDEL [(Lys (K)-Asp (D)-Glu (E)-Leu (L)] endoplasmic reticulum (ER) retention signal (Lee and Luo, 2001). Remarkably, in pre-CW PGs, *mCD8::GFP* is retained intracellularly (Figure 5A and insets) and co-localizes with the ER marker Sec61beta (Summerville et al., 2016), but the GFP signal is clearly cortical post-CW (Figure 5B and insets). In the obese non-pupating *Sema1a*$^{i}$ larvae, the PGs maintain a persistent cytoplasmic *mCD8::GFP* (Figures 5C and 5D and insets).

PLCδ (phospholipase C delta)-PH (pleckstrin homology domain)-EGFP (enhanced green fluorescent protein) (Verstreken et al., 2009) allows to label lipids at the plasma membrane to report phosphatidylinositol 4,5-bisphosphate (PI(4,5)P2) levels *in vivo* (Várnai and Balla, 2006). Analysis revealed extensive expansion of the plasma membrane of mutant PG cells compared with control cells (Figures 5E and 5F), consistent with imbalance in endo/exocytosis in *Sema1a*$^{i}$.

To monitor the secretory capacity of PG cells, we used a secreted GFP protein construct (secGFP; Entchev et al., 2000). In pre-CW PG, secGFP was detected as bright, discrete signals in intracellular granules (Figure 5I and insets), whereas later in the

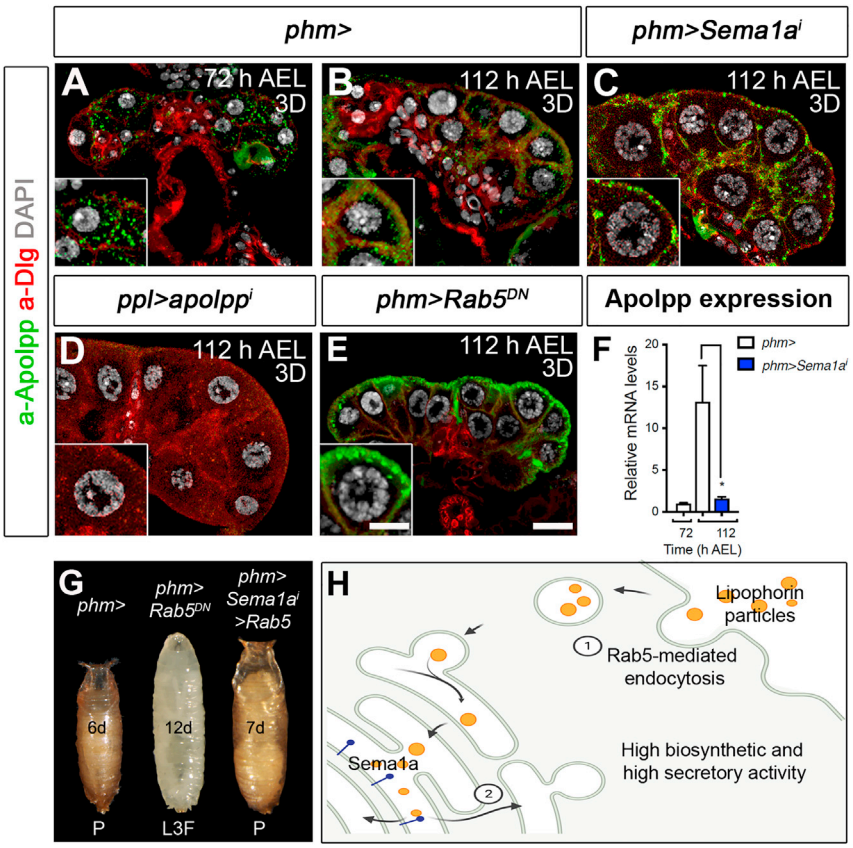


**Figure 4. Internalization of apolpp and endocytosis in CW transition**

(A–C) Apolpp protein (green) within the PG at 72 h (A) and 112 h AEL (B), and retention in the plasma membrane (C) by super-resolution microscopy.

(D) Apolpp labeling in PG from *ppl* > *apolpp*$^{i}$ larvae.

(E) Retention of apolpp at cell membrane in *Rab5*$^{DN}$.

Nuclei (DAPI, gray) and cell membranes (anti-Dlg, red).

(F) *Apolpp* transcripts measured by qRT-PCR.

(G) Larvae *phm* > *Rab5*$^{DN}$ and rescue pupae *phm* > *Sema1a*$^{i}$ > *Rab5*.

(H) Hypothesis of Rab5-mediated lipophorin/apolpp particle uptake leading to the acquisition of biosynthetic and secretory activity in PG cells.

Data are mean ± SEM. *p < 0.05, unpaired t test. Representative larvae or pupae (n = 20). Scale bars, 20 μm; 10 μm (in insets).

actively secreting PGs at wandering stage, cells had low fluorescence distributed in discrete cytoplasmic granules close to the plasma membrane (Figure 5J and insets). The PGs of *Sema1a*$^{i}$ (Figure 5K and insets) and *apolpp*$^{i}$ (Figure 5L and insets) larvae had strong cytoplasmic GFP (quantification in Figure 5M). To accomplish this analysis, we combined *apolpp*$^{i}$ with *phm-Gal4* (note depleting *apolpp* in the PG has no phenotypical consequence; Figure S1E). We verified the defective secretory capacity of *Sema1a*$^{i}$ PG cells by measuring circulating GFP in larval hemolymph (Figure 5N). *Sema1a*$^{i}$ defects were further verified using *Syt::GFP* (Figures 5G and 5H). As expected, *Sema1a*$^{i}$ and *upd2*$^{i}$ larvae fail to produce and secrete ecdysone as seen using ELISA (Figure 5O). Moreover, the size of vesicles containing secGFP was also altered in the fat body in *apolpp*$^{i}$ (Figures S4A–S4C), as expected from the role of apolpp in lipid particle formation (Palm et al., 2012). Collectively, these data clarify events in the acquisition of high secretory capacity (Figure 5P).

## Ribosomal maturation at CW progression

A smooth-to-rough ER transition occurs during the progression from early to mid-third-instar larvae in the PG (Aggarwal and King, 1969; Dai and Gilbert, 1991). At the global level, translation increase during this transition (Church and Robertson, 1966b; Graveley et al., 2011) and a global reduction of ribosomal genes impairs growth in many animal species (Narla and Ebert, 2010). In other insects, ribosomal maturation has been linked to the CW (Lin et al., 2011). Increases in the translation machinery may accelerate protein synthesis in highly demanding conditions, such as those in which enzymes for hormone pulses need to be upregulated.

We noted that the transcription of *Rp49* ribosomal gene increases significantly after CW, but not in *Sema1a*$^{i}$ larvae (Figure S5A). Using Cytoscape 3.8.0 to assemble the Sema1a interaction network based on interactions retrieved from STRING and DroID, we found a significant number of nuclear and ribosomal genes associated with protein translation (e.g., *RpL12*, *RpL9*, *RpS16*, *RpS5b*, *Sbp2*, *eIF3a*, *La*) as gene sets participating in Sema1a-related processes (Figure 6A). A nuclear role is also supported by our findings using a Sema1a antibody (Yu et al., 1998) that Sema1a is prominently localized in the nucleus in a crescent pattern (Figures 6B and S5B), adjacent to the nucleolus (Figures S5E and S5F), and at low levels in the cytoplasm in discrete puncta. The Sema1a protein pattern is not affected by depletion of *apolpp* in the fat body (Figure S5C), but it was absent in *Sema1a* knockdown (Figure S5D).

To functionally link nuclear Sema1a to ribosome biogenesis and protein translation, we used the GFP-tagged large-subunit Ribosomal protein L10a (*GFP-RpL10Ab*; Thomas et al., 2012). In pre-CW, GFP-RpL10Ab remained mainly in the nucleolus (Figure 6C), but after CW, GFP was localized both in the nucleolus and in the cytoplasm (Figure 6D). Surprisingly, overexpression of GFP-RpL10Ab corrected *Sema1a*$^{i}$ defects (Figure 6E) and obesity and maturation arrest (Figure 6F), with 80% (62/77) of animals eclosing as adults. GFP-RpL10Ab overexpression produced by itself a 24- to 26-h puparium delay (Figure 6F). A 10% rescue was observed with the RpL0-like gene, but not with other genes, such as RpL3 or RpS13 (Figure S5G), indicating that RpL10Ab and RpL0-like ribosomal proteins have non-redundant functions in this process.

Consistently, knockdown of *RpL10Ab* (Figure 6F), *RpS3*, *RpS6*, or *RpS13* mimicked *Sema1a*$^{i}$ obese non-pupating phenotypes (Figure S5H). Furthermore, the attainment of CW follows

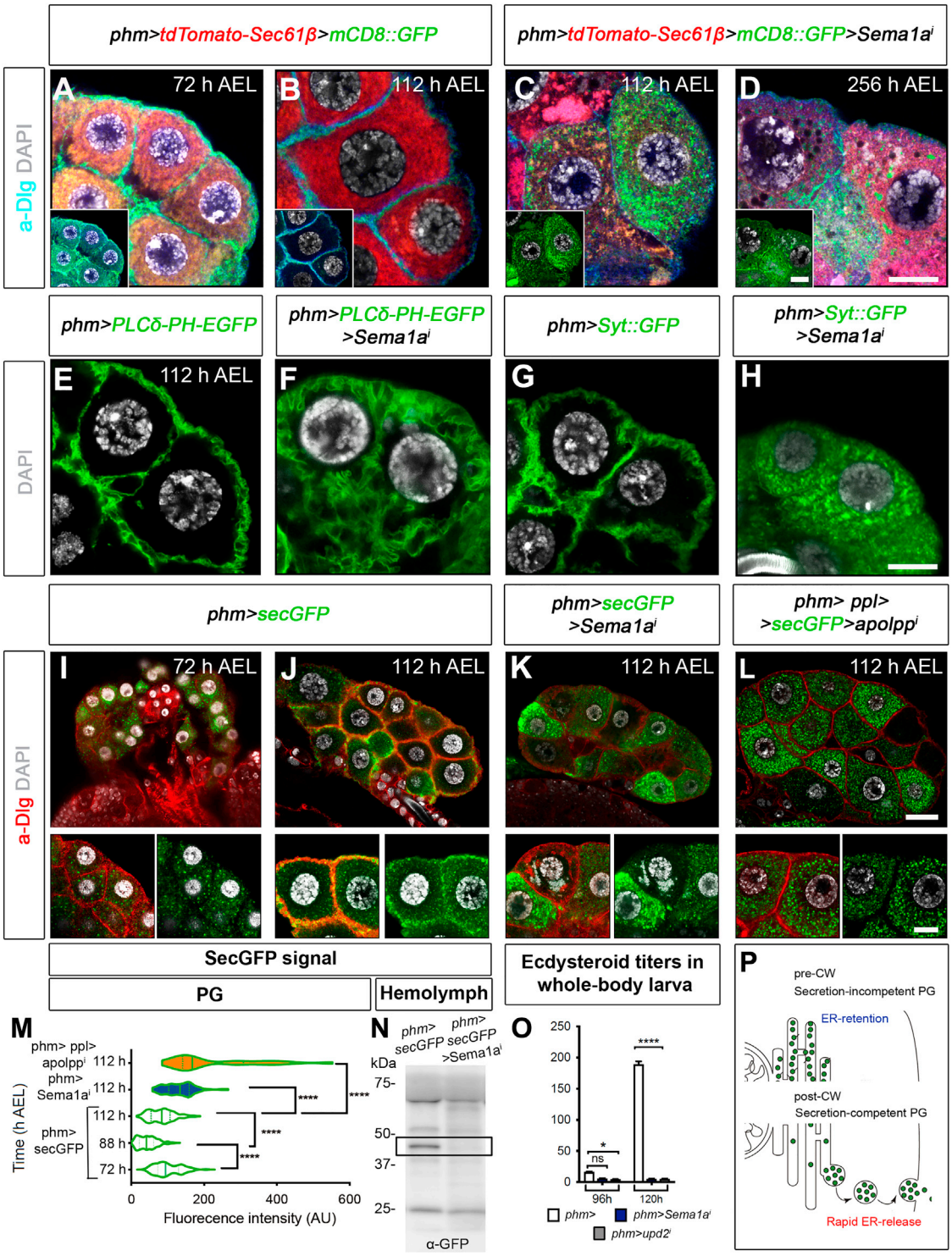


**Figure 5. Fat-derived apolpp in the PG and Sema1a trigger cellular trafficking for secretory competence**

(A and B) Control *phm* > *tdTomato-Sec61β* > *mCD8::GFP* at 72 h (A and inset) and 112 h (B and inset).

(C and D) Cytoplasmic retention of *mCD8::GFP* (inset) in *phm* > *tdTomato-Sec61β* > *mCD8::GFP* > *Sema1a*$^{i}$ at 112 h (C) and 256 h (D). Nuclei (DAPI, gray) and cell membranes (anti-Dlg, blue).

(E and F) Control *phm* > *PLCδ-PH-EGFP* at 112 h (E) and *Sema1a*$^{i}$ at 112 h (F).

(G and H) Control *Syt::GFP* (G) and *Sema1a*$^{i}$ larva at 112 h (H).

*(legend continued on next page)*

an increase in expression of large ribosomal *RpL10Ab* gene, and this increase does not occur in *Sema1a*$^{i}$ mutants (Figure 6G). Taken together, Sema1a mechanistically links transcription and translation control and endocytosis at the CW checkpoint.

### Upd2 and human Leptin downstream of apolpp/Sema1a drive CW progression

The effect of upd2 was validated using three independent *RNA*$^{i}$ lines (Figures 7A and S6A; Table S2). Like *Sema1a*$^{i}$, *phm* > *upd2*$^{i}$ larvae also show a defect in lipogenesis (Figure 7B). This defect, together with our finding that human Leptin expressed in the PG rescues the obese and non-pupation phenotype of *upd2*$^{i}$ larvae (Figure 1A), supports functional homologies in the mechanisms regulating juvenile obesity and sexual maturation. Nonetheless, in flies, upd2 operates from the PG, whereas mammalian Leptin acts primarily from the adipose cells. Leptin is known to be also expressed in the pituitary gland (Gueorguiev et al., 2001), although whether pituitary Leptin has a role in sexual maturation is unknown.

Silencing *upd2* in the fat body results in thinner and smaller flies, owing to defective insulin signaling [(Rajan and Perrimon, 2012 and *ppl* > *upd2*$^{i}$ (Figures 7A and S6A)]. We found that simultaneous silencing of *upd2* in the PG and fat body by *mir-8-Gal4* leads to a combined phenotype: namely, the larvae do not pupate, but they have less fat-body tissue (Figure S6A) as evidenced by their transparency.

Endogenous *upd2* mutant (*upd2*$^{\Delta}$; Hombría et al., 2005) was rescued by overexpression of *upd2* in the PG (Figure 7A). However, the rescued pupae do not progress to adulthood, indicating that the roles of upd2 in the PG and fat body are not entirely redundant, highlighting a more complex role of Leptin-like/upd2 than previously anticipated.

Consistent with previous studies (Rajan and Perrimon, 2012), larvae with reduced *upd2* in the PG also show reduced ILP2 secretion (Figure 2H). However, this mild change seemed to have no functional consequences because systemic IIS was unaffected (Figure S6B), as seen in *Sema1a*$^{i}$ and *apolpp*$^{i}$ larvae. Likewise, as in *Sema1a*$^{i}$ and *apolpp*$^{i}$ mutant larvae, expression levels of *phm* and *dib*, as well as of *E75* (Figure S6C), did not increase in *phm* > *upd2*$^{i}$ larvae.

We found expression of *upd2* (Hombría et al., 2005) in the PG by *phm-Gal4* fully corrected larval obesity and maturation arrest in *Sema1a*$^{i}$ animals (Figure 7A). We also observed that *upd2* overexpression in PGs, but not in the fat body (*ppl>upd2*) (Figure 7A) or in muscles (*twi*, *dmef2* > *upd2*) (Figure S6A), can drive late second/early third instar larvae to prematurely wander out of the food, ~36 h earlier than control larvae (Figure 7A). These small, non-feeding larvae die shortly after, with some having attempted to initiate pupation. Thus, upd2 is both necessary and sufficient to trigger the earliest event in the larval-pupal transition, independent of size.

Overexpression of GFP-RpL10ab in PGs failed to correct the *upd2*$^{i}$ phenotype (Figure 7D). This shows that upd2 expression is required for the translocation of ribosomes from the nucleus. Consistently, expression of human Leptin along with *upd2*$^{i}$ and GFP-RpL10Ab to visualize ribosomes fully rescued the ribosomal translocation (Figure 7E).

Given this finding, we wished to determine whether *upd2* gene expression might itself be a target of Sema1a-mediated CW attainment. Indeed, expression of *upd2* increases after CW, and this increase is not seen in *Sema1a*$^{i}$ mutants, even after 12 days in the feeding stage (Figure 7F).

Mapping the role of upd2 protein across the nucleocytoplasm is challenging, so we attempted to do so using nanobody-based morphotrap technology (Harmansa et al., 2015) to immobilize GFP-tagged upd2. We expected that this would tether upd2 to the membrane, thus impeding its secretion. Surprisingly, we found that upd2::GFP was trapped in the nuclei of PG cells (Figure 7G), and that the nanobody-based trapping of upd2::GFP led to a non-pupating and massively obese phenotype that was indistinguishable from *phm* > *upd2*$^{i}$ larvae (Figure S6A). Together, upd2 secretion by PG cells is essential for signaling the transition through the CW point, and important events of the trigger for this transition are in the nucleus.

## DISCUSSION

Prepubertal juveniles tend to maximize food intake to sustain their rapid growth, and they store excess energy as fat to promote survival in times of fasting and reproductive capacity in the adult stage (Kaplowitz, 2008; Tu and Tatar, 2003). Our study illustrates that the defect in the decision to mature can result as a "side effect" of persistent and maladaptive responses that could explain the progressive obesity associated with failure to enter puberty in children with conditions such as Prader-Willi syndrome or *Leptin/LepR* deficiency or resistance. Specifically, our data suggest that the inability to monitor body-fat stores in young animals not only prevents their entry into puberty but also has the effect of continued fat deposition. The inability to monitor fat stores may also explain why these animals are not satiated and show chronic feeding (Figure 7H). Our data further highlight the potential of steroid hormone supplementation to limit juvenile obesity in cases of *Leptin* deficiency or resistance.

### The steroidogenic gland as a source of Leptin-like upd2 to signal the "sufficiency" of body fat to initiate maturation

The decision-making process about sexual maturation is closely related to a nutrient-associated behavior switch that leads to the "commitment" pulse of ecdysone (Berreur et al.,

(I–L) Control *phm>secGFP* at 72 h (I) and 112 h (J), and *Sema1a*$^{i}$ larva (K) and a *phm* > *ppl* > *apolpp*$^{i}$ larva (L) at 112 h. DAPI-labeled nuclei (gray) and cell membranes (anti-Dlg, red).
(M) Violin plots of secGFP cytoplasmic content measured using ImageJ.
(N) Western blot of the hemolymph secGFP protein in the indicated genotypes at 112 h.
(O) Whole-body 20E levels in *phm>* larvae and in *Sema1a*$^{i}$ and *upd2*$^{i}$ larvae at 96 and 120 h were measured by ELISA.
(P) Schematic of ER retention/release of *secGFP*.
Data are mean ± SEM. *p < 0.05, **p < 0.01, ***p < 0.001, ****p < 0.0001, one-way ANOVA (M) and two-way ANOVA (O). Scale bars, 10 μm, except 20 μm in high magnifications in I–L. All are super-resolution images.

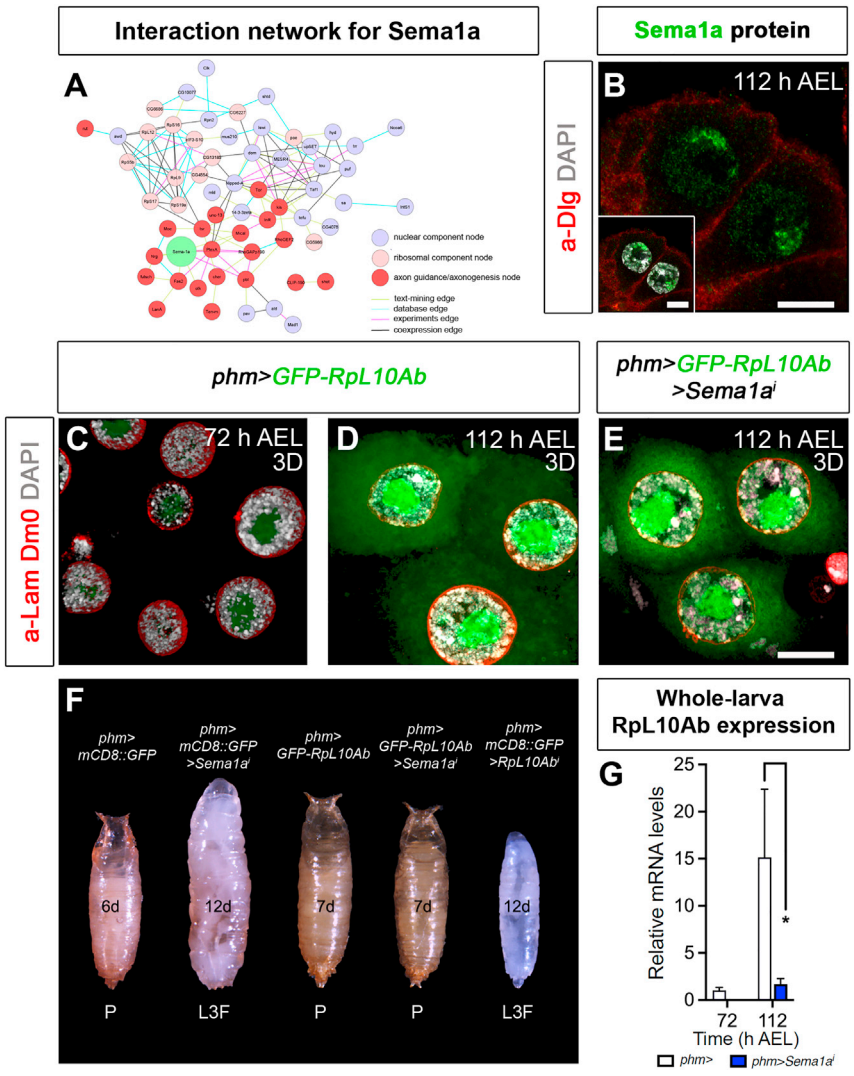


**Figure 6. Regulation of PG maturation and sexual commitment by ribosomal protein L10Ab**

(A) Interaction network for Sema1a (green). Circles highlight genes for axonogenesis (red), translation initiation and ribosomes (pink), and nuclear signaling (purple).

(B–E) Super-resolution images. (B) Control PG at 112 h stained with anti-Sema1a (green). Nuclei (DAPI, gray) and cell membranes (anti-Dlg, red). (C–E) 3D reconstructions of GFP-RpL10Ab in control (C and D) and *Sema1a*$^{i}$ (E). Nuclear lamina (anti-Lam Dm0, red) and nuclei (DAPI, gray).

(F) Representative animals (n = 20) are shown.

(G) qRT-PCR analysis of *RpL10Ab*.

Data are mean ± SEM. *p < 0.05, unpaired t test. Scale bars, 10 μm.

1979; Nijhout and Williams, 1974). Our study also finds that upd2 and its human homolog Leptin produced by the PG cells triggers events previously attributed exclusively to the surges of ecdysone and similar to those in mammals (Han et al., 2020). *Upd2* transcription is regulated by carbohydrates and lipids (Rajan and Perrimon, 2012), and here we show that *upd2* increases upon lipid sensing in a switch-like manner at CW to signal the end of the feeding period and initiation of maturation along with ecdysone (Figure 7F). Importantly, both fly upd2 and human Leptin are sufficient to cause premature cessation of feeding by 36 h, suggesting upd2 acts upstream or in parallel to ecdysone.

The finding that PG is important for the control of feeding, body weight, and upd2-mediated sexual maturation and its rescue by human Leptin is of great interest. For example, obesity and non-pupating *phm > upd2*$^{i}$ is like that of the classical Leptin mutant phenotype (Clément et al., 1998; Friedman and Halaas, 1998; Montague et al., 1997). Upd2 acting in different tissues, along with redundancy between *upd* genes, may explain the viability of animals with *upd2* mutations, as well as the fact that a loss of fat-body-derived upd2 hinders the obesity effects. Another cytokine, upd1, acting in the brain was also proposed as the actual Leptin that inhibits body weight (Beshel et al., 2017). Our data support upd2 as the fly Leptin and identify the PG as a key site for body weight control in juveniles.

Upd2 in the PG appears to be required earlier than in the fat body, and this could be a difference between our study and previous studies. Studies by Fujikawa et al. (2013) in a mouse model of insulin deficiency diabetes suggest that the connection between Leptin and insulin could be complicated. In those mice, LepR in GABA neurons mimicked the antidiabetic actions of insulin. Upd2 could mimic ILP defects, but these effects could occur in reality without changes in ILPs or without acting via ILPs. Our study supports that possible scenario. Although loss of IIS in the PG produces non-pupating phenotypes, the phenotype of *upd2*$^{i}$ does seem to occur through the systemic alteration of IIS because activation of IIS and TOR at different steps of these pathways fails to rescue pupation.

## Lipid carrier apolpp and Sema1a form a bidirectional circuit upstream of Leptin/upd2

The lipid carrier and transporters, apolpp and Fatp2, demonstrate the fundamental role of lipids in the maturation decision-making process. Apolpp secreted in proportion to the amount of stored fat by fat cells (Palm et al., 2012) is a strong candidate to directly deliver adiposity information. Uptake of apolpp by Rab5-mediated endocytosis is fundamental for the decision to enter metamorphosis. Furthermore, downstream of this event is a dramatic remodeling of endomembrane that occurs at the CW transition. We reasoned that the entry of lipids and/or apolpp

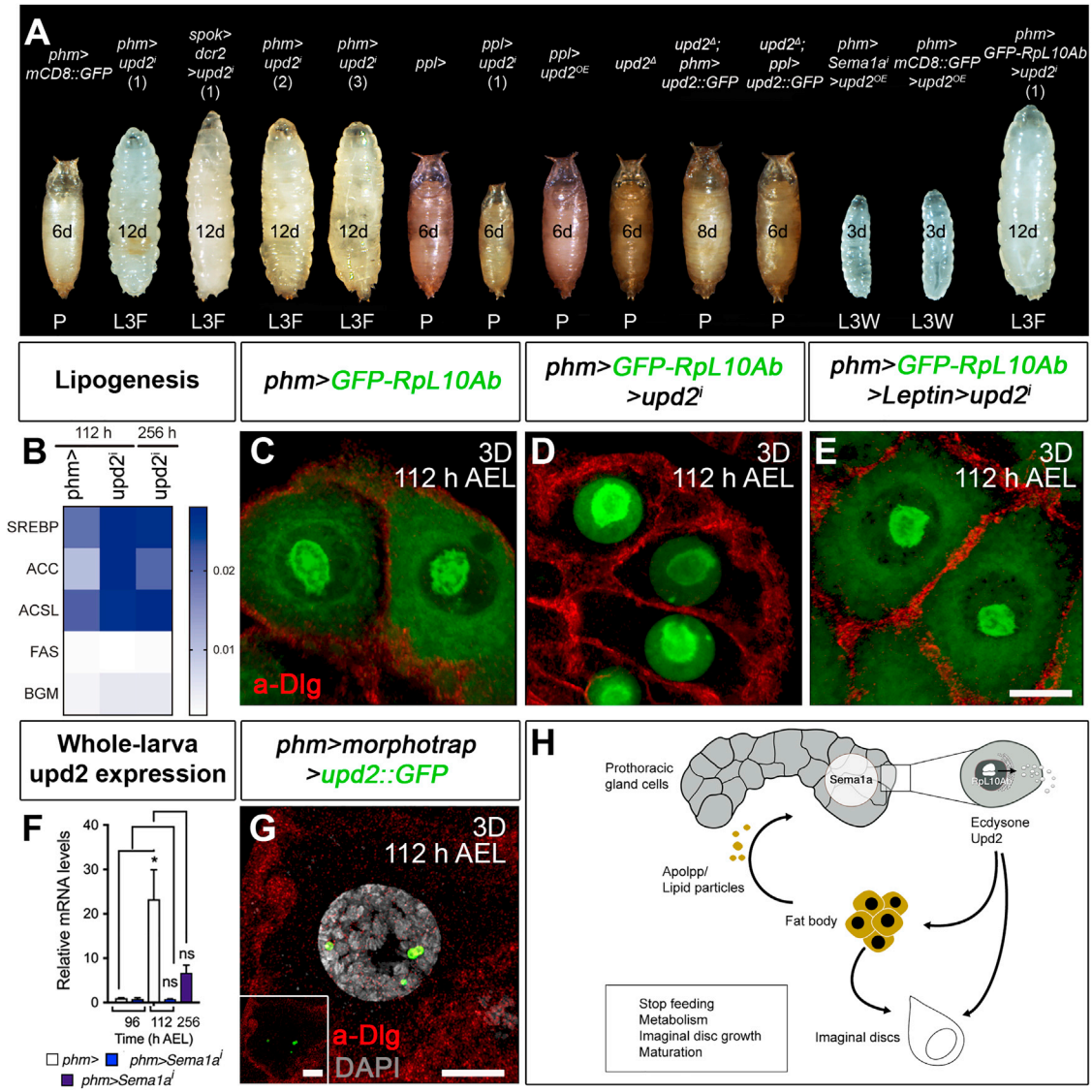


**Figure 7. Upd2 acts downstream of the apolpp/Sema1a/RpL10Ab axis**

(A) Shown are representative animals (n = 20 per genotype) of indicated genotypes and ages. The *upd2 RNA*$^{i}$ lines are *RNAi#1* (*HMS00901*, BDSC #*33949*), *RNAi#2* (*5988R-1*), and *RNAi#3* (*5988R-3*).

(B) Heatmap of qRT-PCR data.

(C–E) 3D reconstructions of *GFP-RpL10Ab* in control (C), *upd2*$^{i}$ (D), and *Leptin* > *upd2*$^{i}$ (E). Cell membranes (anti-Dlg, red).

(F) *upd2* transcript levels measured by qRT-PCR.

(G) 3D reconstruction of a PG cell with overexpression of *upd2* and morphotrap (*phm* > *upd2::GFP* > *VHH-GFP4::CD8::mCherry*). Nuclei (DAPI, gray) and cell membranes (anti-Dlg, red).

(H) Model for two-way communication between adipose tissue and PG for sexual maturation commitment. Upon Rab5-dependent macropinocytosis and endocytosis uptake of lipids/apolpp and other circulating proteins and nutrients, Sema1a at the PG triggers events leading to acquisition of high biosynthetic and secretory capacity via nucleocytoplasmic traffic and of ribosomes maturation. Data are mean ± SEM. *p < 0.05, unpaired t test. Scale bars, 10 μm.

may help this process via a yet unclear nuclear Sema1a process. Alternatively, apolpp may serve only as a scaffold to transport lipids or lipophilic signals into the PG cells without the need to interact with the Sema1a-dependent sensor. Sema1a at the nuclear membrane could "sense" variations in the composition of the membrane because of the incorporation of lipids, leading to the transport of ribosomes across the nuclear pores. Once the ribosomes are assembled in the ER, the PG cells can acquire a high biosynthetic activity to produce high levels of *Halloween* genes and *upd2* and other genes. At the same time, changes in the ER membranes (probably also as a result of lipid incorporation) could release the "brake" and initiate secretion. We hypothesize that these events enable the production of peaks of ecdysone and upd2 (Figure 7H).

### Endocytosis of apolpp is required upstream of endomembrane remodeling

Much of the work on CW has focused on the regulation of the expression of *Halloween* genes (Yamanaka et al., 2013) and the mechanisms of ecdysone secretion (Yamanaka et al., 2015). We extend these findings showing how nutrition may trigger the secretory activity of the gland upstream of these events and how secretion and biosynthesis are coupled.

Super-resolution imaging of PG uncovers that a signal retains newly synthesized proteins, and probably other cargo in the ER before CW, also revealing that gland cells are secretion incompetent at this stage and had low biosynthetic activity (Figure 5P). We also document dramatic remodeling in the ER preceding the acquisition of high secretory activity consistent with earlier ultrastructural studies (Aggarwal and King, 1969; Dai and Gilbert, 1991). These earlier observations also hinted that pre-CW is dominated by macropinocytosis, a regulated form of endocytosis. It seems logical that PG cells prioritize the uptake of circulating secreted factors, lipid particles, and other nutrients, until they are capable of synthesizing large amounts of hormone to produce peaks (rather than tonic release) of hormones. Our data uncover a secretion ''brake'' that prevents the trafficking of secretory and membrane proteins and other cargo from the ER to the plasma membranes, which is Sema1a dependent. In mammals, pulsatile hormone release is critical for the proper function of the maturation axis, as well as the reproductive axis in adults.

### Nuclear Sema1a and nucleocytoplasmic transport for signaling ecdysone synthesis

Peripheral fat levels are ultimately sensed in the nucleus, where the transcription of ecdysone biosynthetic genes begins. Interestingly, nucleocytoplasmic transport precedes, and is a prerequisite for, ecdysone biosynthesis (Figure 1I). In mice, mutations in *Sema4A* result in defects in protein trafficking, leading to retinal degeneration (Nojima et al., 2013). This suggests that trafficking may be a conserved role of semaphorins.

Sema1a is in the nuclear envelope, which is in a continuum with the ER, the Golgi apparatus, and lysosomes, and it communicates with the plasma membrane via endocytosis and exocytosis. Using a GFP-fused RpL10Ab, we discovered regulated nucleocytoplasm trafficking of immature ribosome at the CW transition, which is blocked in the *Sema1a* and *apolpp* deficiency, as well as in *upd2* mutants, as seen clearly in the *upd2*$^{i}$ unrescued animals. RpL10Ab-apolpp highlights the importance of lipid transport for nucleocytoplasmic trafficking and ribosome maturation as key events for the sexual maturation decision-making process (Figure 7H).

Not only Sema1a but also human SEMA3E, SEMA4A, and SEMA6A are prominently localized to the nucleus and in discrete puncta in the ER (Thul et al., 2017). Moreover, fat sensors are often multi-pass membrane proteins (Holmer and Worman, 2001; Romanauska and Köhler, 2018), and Sema1a has two predicted transmembrane domains (https://www.uniprot.org/uniprot/Q24322). We speculate that lipid-sensing mediating proteolysis or rotation along the membrane could facilitate trafficking of Sema1a or other semaphorin proteins from the nuclear membrane to the ER as we had seen post-CW.

Recently, it has been shown that the inner nuclear membrane is an active metabolic site for phospholipid synthesis and sensors (Holmer and Worman, 2001). Nuclear integral transmembrane proteins are synthesized in the ER and may diffuse freely from the ER to the inner nuclear membrane, where they are retained through association with nuclear ligands (Romanauska and Köhler, 2018). We hypothesized that ''activation'' of Sema1a may occur only when it is released from the nuclear membrane. More speculatively, this activation may be direct via an apolpp, because Sema1a and apolpp proteins physically interact in embryos (Rees et al., 2011).

### Long-chain fatty acid transport and CW attainment

Lipids are essential components of cell membranes, and lipid changes during development, at both the organism (Guan et al., 2013) and organ level (Carvalho et al., 2012), but information about lipid composition in the PG was not resolved in those studies. Fatp2 transports long-chain fatty acid and is shown here to be essential for the larval-to-pupal transition. In mammalian cells, FATP-dependent uptake of lipids occurs in response to insulin, providing a possible link between IIS/TOR and apolpp/Sema1a-mediated processes.

Diet is known to impact lipid composition (Carvalho et al., 2012) and, consistent with our data, Musselman et al. (2011) reported that feeding larvae with a fat-rich diet, but not a high-sugar or protein-rich diet, slightly accelerates metamorphosis. Dietary lipids are transported by lipophorin particles, which explains how apolpp influences the onset of maturation.

Collectively, our data firmly link the maturation decision-making process to fat sensing and some forms of juvenile obesity. Because *SEMA3* variants occur in morbid obesity and affect the development or maturation of hypothalamic circuits in fish (van der Klaauw et al., 2019), our findings may go beyond *Drosophila*.

## STAR★METHODS

Detailed methods are provided in the online version of this paper and include the following:

- KEY RESOURCES TABLE
- RESOURCE AVAILABILITY
  - Lead contact
  - Materials availability
  - Data and code availability
- EXPERIMENTAL MODEL AND SUBJECT DETAILS
  - *Drosophila* Husbandry
  - Screenings of Nutrient Transporters, Secreted and Transmembrane Factors by RNA$^{i}$
- METHOD DETAILS
  - Measurement of the Developmental Timing of Pupation
  - Immunohistochemistry in Larval Imaginal Discs, Fat bodies and Brains
  - Super-resolution Confocal Imaging of Larval Brains, Fat Bodies and Prothoracic Gland Cells
  - Neutral Lipid Staining and Quantification in Larval Brains
  - Bromophenol Blue Incorporation

## SUPPLEMENTAL INFORMATION

Supplemental information can be found online at https://doi.org/10.1016/j.celrep.2021.109830.

## ACKNOWLEDGMENTS

We thank M. Affolter, F. Azorin, H. Bellen, M. Brankatschk, G. Bashaw, A. Carmena, F. Casares, J. Castelli, J. Culi, B. Edgar, A. Kolodkin, B. Hassan, P. Leopold, L. Luo, N. Perrimon, H. Stocker, and K. Rewitz for reagents. We also thank the Bloomington Stock Center (NIH P40OD018537), the TRiP at Harvard Medical School (NIH/NIGMS R01-GM084947), the NIG and the Kyoto Stock Center for providing fly stocks, and the Developmental Studies Hybridoma Bank at the University of Iowa for antibodies. Figure 4H and the graphical abstract were created with BioRender.com. We also thank G. Exposito and V. Villar for assistance with Airyscan microscopy, S. Javaloy for helping with illustrations, and L. Mira for assistance in fly stock keeping. This work was supported by Generalitat Valenciana Grant co-financed with European Regional Development Fund (OP ERDF of Comunitat Valenciana 2014-2020) to M.-P.S. and by Spanish National Grant (PID2020-115875RB-I00) to A.P.-L. The Spanish National Grants (BFU2015-64239-R and PID2019-106002RB-I00) were co-financed by the ERDF, the Fundación Científica Española Contra el Cáncer (AECC) (CICPF16001DOMÍ), and Generalitat Valenciana Grant (PROMETEO/2017/146) (to M.D.). J.M. was financed by the Ramon y Cajal Program (RyC-2010-07155), a Spanish National Grant (BFU2016-76295-R) co-financed by the ERDF, and a CSIC grant (2019AEP181). M.D. and J.M. were also funded by the "Severo Ochoa" Program for Centers of Excellence in R&D (SEV-2017-0723) co-financed by ERDF. P.R.-C., J.C.-V., R.S., and S.J.-C. are Spanish doctoral FPI fellows (BES-2013-062980, BES-2017-081122, BES-2016-077689, and BES-2013-064947, respectively) from the Spanish Ministerio de Economia y Competitividad.

## AUTHOR CONTRIBUTIONS

Conceptualization and data analysis, J.M. and M.D.; methodology, J.M., M.D., M.P.-S., and A.P.-L.; investigation, J.M., S.J.-C., D.M.V., J.C.-V., M.P.-S., P.R.-C., R.S., E.d.H., D.F.-M., A.R., H.P.P., and E.B.-I.; writing – original draft, J.M. and M.D.; writing – review & editing, J.M. and M.D.; funding acquisition, J.M., M.D., M.P.-S., and A.P.-L.; supervision, J.M. and M.D.

## DECLARATION OF INTERESTS

The authors declare no competing interests.

## INCLUSION AND DIVERSITY

We worked to ensure sex balance in the selection of non-human subjects. One or more of the authors of this paper self-identifies as a member of the LGBTQ+ community. While citing references scientifically relevant for this work, we also actively worked to promote gender balance in our reference list.

Received: August 3, 2020
Revised: June 25, 2021
Accepted: September 23, 2021
Published: October 12, 2021

## REFERENCES

Aggarwal, S.K., and King, R.C. (1969). A comparative study of the ring glands from wild type and 1(2)gl mutant Drosophila melanogaster. J. Morphol. *129*, 171–199.

Ahmed, M.L., Ong, K.K., and Dunger, D.B. (2009). Childhood obesity and the timing of puberty. Trends Endocrinol. Metab. *20*, 237–242.

Alto, L.T., and Terman, J.R. (2017). Semaphorins and their Signaling Mechanisms. Methods Mol. Biol. *1493*, 1–25.

Andres, A.J., Fletcher, J.C., Karim, F.D., and Thummel, C.S. (1993). Molecular analysis of the initiation of insect metamorphosis: a comparative study of Drosophila ecdysteroid-regulated transcription. Dev. Biol. *160*, 388–404.

Arrese, E.L., and Soulages, J.L. (2010). Insect fat body: energy, metabolism, and regulation. Annu. Rev. Entomol. *55*, 207–225.

Arrese, E.L., Canavoso, L.E., Jouni, Z.E., Pennington, J.E., Tsuchida, K., and Wells, M.A. (2001). Lipid storage and mobilization in insects: current status and future directions. Insect Biochem. Mol. Biol. *31*, 7–17.

Bader, R., Sarraf-Zadeh, L., Peters, M., Moderau, N., Stocker, H., Köhler, K., Pankratz, M.J., and Hafen, E. (2013). The IGFBP7 homolog Imp-L2 promotes insulin signaling in distinct neurons of the Drosophila brain. J. Cell Sci. *126*, 2571–2576.

Baker, E.R. (1985). Body weight and the initiation of puberty. Clin. Obstet. Gynecol. *28*, 573–579.

Bellaïche, Y., Gho, M., Kaltschmidt, J.A., Brand, A.H., and Schweisguth, F. (2001). Frizzled regulates localization of cell-fate determinants and mitotic spindle rotation during asymmetric cell division. Nat. Cell Biol. *3*, 50–57.

Berreur, P., Porcheron, P., Berreur-Bonnenfant, J., and Simpson, P. (1979). Ecdysteroid levels and pupariation in Drosophila melanogaster. J. Exp. Zool. *210*, 347–352.

Beshel, J., Dubnau, J., and Zhong, Y. (2017). A Leptin Analog Locally Produced in the Brain Acts via a Conserved Neural Circuit to Modulate Obesity-Linked Behaviors in Drosophila. Cell Metab. *25*, 208–217.

Blazsek, I., and Mala, J. (1978). Steroid transport through the surface of the prothoracic gland cells in Galleria mellonella L. Cell Tissue Res. *187*, 507–513.

Bloomfield, G., and Kay, R.R. (2016). Uses and abuses of macropinocytosis. J. Cell Sci. *129*, 2697–2705.

Brankatschk, M., and Eaton, S. (2010). Lipoprotein particles cross the blood-brain barrier in Drosophila. J. Neurosci. *30*, 10441–10447.

Caldwell, P.E., Walkiewicz, M., and Stern, M. (2005). Ras activity in the Drosophila prothoracic gland regulates body size and developmental rate via ecdysone release. Curr. Biol. *15*, 1785–1795.

Carvalho, M., Sampaio, J.L., Palm, W., Brankatschk, M., Eaton, S., and Shevchenko, A. (2012). Effects of diet and development on the Drosophila lipidome. Mol. Syst. Biol. *8*, 600.

Chen, X., and Dickman, D. (2017). Development of a tissue-specific ribosome profiling approach in Drosophila enables genome-wide evaluation of translational adaptations. PLoS Genet. *13*, e1007117.

Church, R.B., and Robertson, F.W. (1966a). Biochemical analysis of genetic differences in the growth of Drosophila. Genet. Res. *7*, 383–407.

Church, R.B., and Robertson, F.W. (1966b). A biochemical study of the growth of Drosophila melanogaster. J. Exp. Zool. *162*, 337–351.

Clément, K., Vaisse, C., Lahlou, N., Cabrol, S., Pelloux, V., Cassuto, D., Gourmelen, M., Dina, C., Chambaz, J., Lacorte, J.M., et al. (1998). A mutation in the human leptin receptor gene causes obesity and pituitary dysfunction. Nature *392*, 398–401.

Colombani, J., Bianchini, L., Layalle, S., Pondeville, E., Dauphin-Villemant, C., Antoniewski, C., Carré, C., Noselli, S., and Léopold, P. (2005). Antagonistic actions of ecdysone and insulins determine final size in Drosophila. Science *310*, 667–670.

Cruz, J., Martín, D., and Franch-Marro, X. (2020). Egfr Signaling Is a Major Regulator of Ecdysone Biosynthesis in the Drosophila Prothoracic Gland. Curr. Biol. *30*, 1547–1554.e4.

Dai, J.D., and Gilbert, L.I. (1991). Metamorphosis of the corpus allatum and degeneration of the prothoracic glands during the larval-pupal-adult transformation of Drosophila melanogaster: a cytophysiological analysis of the ring gland. Dev. Biol. *144*, 309–326.

Dietzl, G., Chen, D., Schnorrer, F., Su, K.C., Barinova, Y., Fellner, M., Gasser, B., Kinsey, K., Oppel, S., Scheiblauer, S., et al. (2007). A genome-wide transgenic RNAi library for conditional gene inactivation in Drosophila. Nature *448*, 151–156.

Eijkelenboom, A., and Burgering, B.M. (2013). FOXOs: signalling integrators for homeostasis maintenance. Nat. Rev. Mol. Cell Biol. *14*, 83–97.

Entchev, E.V., Schwabedissen, A., and González-Gaitán, M. (2000). Gradient formation of the TGF-beta homolog Dpp. Cell *103*, 981–991.

Friedman, J.M., and Halaas, J.L. (1998). Leptin and the regulation of body weight in mammals. Nature *395*, 763–770.

Frisch, R.E., and Revelle, R. (1970). Height and weight at menarche and a hypothesis of critical body weights and adolescent events. Science *169*, 397–399.

Fujikawa, T., Berglund, E.D., Patel, V.R., Ramadori, G., Vianna, C.R., Vong, L., Thorel, F., Chera, S., Herrera, P.L., Lowell, B.B., et al. (2013). Leptin engages a hypothalamic neurocircuitry to permit survival in the absence of insulin. Cell Metab. *18*, 431–444.

Garelli, A., Gontijo, A.M., Miguela, V., Caparros, E., and Dominguez, M. (2012). Imaginal discs secrete insulin-like peptide 8 to mediate plasticity of growth and maturation. Science *336*, 579–582.

Gibbens, Y.Y., Warren, J.T., Gilbert, L.I., and O'Connor, M.B. (2011). Neuroendocrine regulation of Drosophila metamorphosis requires TGFbeta/Activin signaling. Development *138*, 2693–2703.

Graveley, B.R., Brooks, A.N., Carlson, J.W., Duff, M.O., Landolin, J.M., Yang, L., Artieri, C.G., van Baren, M.J., Boley, N., Booth, B.W., et al. (2011). The developmental transcriptome of Drosophila melanogaster. Nature *471*, 473–479.

Grönke, S., Mildner, A., Fellert, S., Tennagels, N., Petry, S., Müller, G., Jäckle, H., and Kühnlein, R.P. (2005). Brummer lipase is an evolutionary conserved fat storage regulator in Drosophila. Cell Metab. *1*, 323–330.

Guan, X.L., Cestra, G., Shui, G., Kuhrs, A., Schittenhelm, R.B., Hafen, E., van der Goot, F.G., Robinett, C.C., Gatti, M., Gonzalez-Gaitan, M., and Wenk, M.R. (2013). Biochemical membrane lipidomics during Drosophila development. Dev. Cell *24*, 98–111.

Gueorguiev, M., Góth, M.L., and Korbonits, M. (2001). Leptin and puberty: a review. Pituitary *4*, 79–86.

Han, X., Burger, L.L., Garcia-Galiano, D., Sim, S., Allen, S.J., Olson, D.P., Myers, M.G., Jr., and Elias, C.F. (2020). Hypothalamic and Cell-Specific Transcriptomes Unravel a Dynamic Neuropil Remodeling in Leptin-Induced and Typical Pubertal Transition in Female Mice. iScience *23*, 101563.

Harmansa, S., Hamaratoglu, F., Affolter, M., and Caussinus, E. (2015). Dpp spreading is required for medial but not for lateral wing disc growth. Nature *527*, 317–322.

Hernandez-Fleming, M., Rohrbach, E.W., and Bashaw, G.J. (2017). Sema-1a Reverse Signaling Promotes Midline Crossing in Response to Secreted Semaphorins. Cell Rep. *18*, 174–184.

Hobson, R.P. (1935). On a fat-soluble growth factor required by blow-fly larvae: Identity of the growth factor with cholesterol. Biochem. J. *29*, 2023–2026.

Holmer, L., and Worman, H.J. (2001). Inner nuclear membrane proteins: functions and targeting. Cell. Mol. Life Sci. *58*, 1741–1747.

Hombría, J.C., Brown, S., Häder, S., and Zeidler, M.P. (2005). Characterisation of Upd2, a Drosophila JAK/STAT pathway ligand. Dev. Biol. *288*, 420–433.

Igarashi, F., Ogihara, M.H., Iga, M., and Kataoka, H. (2018). Cholesterol internalization and metabolism in insect prothoracic gland, a steroidogenic organ, via lipoproteins. Steroids *134*, 110–116.

Jeong, S., Juhaszova, K., and Kolodkin, A.L. (2012). The control of semaphorin-1a-mediated reverse signaling by opposing pebble and RhoGAPp190 functions in Drosophila. Neuron *76*, 721–734.

Känsäkoski, J., Fagerholm, R., Laitinen, E.M., Vaaralahti, K., Hackman, P., Pitteloud, N., Raivio, T., and Tommiska, J. (2014). Mutation screening of SEMA3A and SEMA7A in patients with congenital hypogonadotropic hypogonadism. Pediatr. Res. *75*, 641–644.

Kaplowitz, P.B. (2008). Link between body fat and the timing of puberty. Pediatrics *121* (*Suppl 3*), S208–S217.

Karim, F.D., and Rubin, G.M. (1998). Ectopic expression of activated Ras1 induces hyperplastic growth and increased cell death in Drosophila imaginal tissues. Development *125*, 1–9.

Katz, M.G., and Vollenhoven, B. (2000). The reproductive endocrine consequences of anorexia nervosa. BJOG *107*, 707–713.

Kennedy, G.C., and Mitra, J. (1963). Body weight and food intake as initiating factors for puberty in the rat. J. Physiol. *166*, 408–418.

Kiral, F.R., Kohrs, F.E., Jin, E.J., and Hiesinger, P.R. (2018). Rab GTPases and Membrane Trafficking in Neurodegeneration. Curr. Biol. *28*, R471–R486.

Koyama, T., and Mirth, C.K. (2021). Ecdysone Quantification from Whole Body Samples of *Drosophila melanogaster* Larvae. Bio. Protoc. *11*, e3915.

Koyama, T., Rodrigues, M.A., Athanasiadis, A., Shingleton, A.W., and Mirth, C.K. (2014). Nutritional control of body size through FoxO-Ultraspiracle mediated ecdysone biosynthesis. eLife *3*, e03091.

Kunte, A.S., Matthews, K.A., and Rawson, R.B. (2006). Fatty acid auxotrophy in Drosophila larvae lacking SREBP. Cell Metab. *3*, 439–448.

Kutty, R.K., Kutty, G., Kambadur, R., Duncan, T., Koonin, E.V., Rodriguez, I.R., Odenwald, W.F., and Wiggert, B. (1996). Molecular characterization and developmental expression of a retinoid- and fatty acid-binding glycoprotein from Drosophila. A putative lipophorin. J. Biol. Chem. *271*, 20641–20649.

Layalle, S., Arquier, N., and Léopold, P. (2008). The TOR pathway couples nutrition and developmental timing in Drosophila. Dev. Cell *15*, 568–577.

Lee, T., and Luo, L. (2001). Mosaic analysis with a repressible cell marker (MARCM) for Drosophila neural development. Trends Neurosci. *24*, 251–254.

Li, L., Edgar, B.A., and Grewal, S.S. (2010). Nutritional control of gene expression in Drosophila larvae via TOR, Myc and a novel cis-regulatory element. BMC Cell Biol. *11*, 7.

Lin, J.I., Mitchell, N.C., Kalcina, M., Tchoubrieva, E., Stewart, M.J., Marygold, S.J., Walker, C.D., Thomas, G., Leevers, S.J., Pearson, R.B., et al. (2011). Drosophila ribosomal protein mutants control tissue growth non-autonomously via effects on the prothoracic gland and ecdysone. PLoS Genet. *7*, e1002408.

Lockett, T.J., and Ashburner, M. (1989). Temporal and spatial utilization of the alcohol dehydrogenase gene promoters during the development of Drosophila melanogaster. Dev. Biol. *134*, 430–437.

Mattila, J., and Hietakangas, V. (2017). Regulation of Carbohydrate Energy Metabolism in *Drosophila melanogaster*. Genetics *207*, 1231–1253.

McBrayer, Z., Ono, H., Shimell, M., Parvy, J.P., Beckstead, R.B., Warren, J.T., Thummel, C.S., Dauphin-Villemant, C., Gilbert, L.I., and O'Connor, M.B. (2007). Prothoracicotropic hormone regulates developmental timing and body size in Drosophila. Dev. Cell *13*, 857–871.

McGuire, S.E., Le, P.T., Osborn, A.J., Matsumoto, K., and Davis, R.L. (2003). Spatiotemporal rescue of memory dysfunction in Drosophila. Science *302*, 1765–1768.

Mirth, C.K., and Riddiford, L.M. (2007). Size assessment and growth control: how adult size is determined in insects. BioEssays *29*, 344–355.

Mirth, C., Truman, J.W., and Riddiford, L.M. (2005). The role of the prothoracic gland in determining critical weight for metamorphosis in Drosophila melanogaster. Curr. Biol. *15*, 1796–1807.

Moeller, M.E., Nagy, S., Gerlach, S.U., Soegaard, K.C., Danielsen, E.T., Texada, M.J., and Rewitz, K.F. (2017). Warts Signaling Controls Organ and Body Growth through Regulation of Ecdysone. Curr. Biol. *27*, 1652–1659.e4.

Montague, C.T., Farooqi, I.S., Whitehead, J.P., Soos, M.A., Rau, H., Wareham, N.J., Sewter, C.P., Digby, J.E., Mohammed, S.N., Hurst, J.A., et al. (1997). Congenital leptin deficiency is associated with severe early-onset obesity in humans. Nature *387*, 903–908.

Morante, J., and Desplan, C. (2011). Dissection and staining of Drosophila optic lobes at different stages of development. Cold Spring Harb. Protoc. *2011*, 652–656.

Morante, J., Vallejo, D.M., Desplan, C., and Dominguez, M. (2013). Conserved miR-8/miR-200 defines a glial niche that controls neuroepithelial expansion and neuroblast transition. Dev. Cell *27*, 174–187.

Musselman, L.P., Fink, J.L., Narzinski, K., Ramachandran, P.V., Hathiramani, S.S., Cagan, R.L., and Baranski, T.J. (2011). A high-sugar diet produces obesity and insulin resistance in wild-type Drosophila. Dis. Model. Mech. *4*, 842–849.

Nagarajan, S., and Grewal, S.S. (2014). An investigation of nutrient-dependent mRNA translation in Drosophila larvae. Biol. Open *3*, 1020–1031.

Nagarkar-Jaiswal, S., Lee, P.T., Campbell, M.E., Chen, K., Anguiano-Zarate, S., Gutierrez, M.C., Busby, T., Lin, W.W., He, Y., Schulze, K.L., et al. (2015). A library of MiMICs allows tagging of genes and reversible, spatial and temporal knockdown of proteins in Drosophila. eLife *4*, e05338.

Narla, A., and Ebert, B.L. (2010). Ribosomopathies: human disorders of ribosome dysfunction. Blood *115*, 3196–3205.

Ni, J.Q., Zhou, R., Czech, B., Liu, L.P., Holderbaum, L., Yang-Zhou, D., Shim, H.S., Tao, R., Handler, D., Karpowicz, P., et al. (2011). A genome-scale shRNA resource for transgenic RNAi in Drosophila. Nat. Methods *8*, 405–407.

Nijhout, H.F., and Williams, C.M. (1974). Control of moulting and metamorphosis in the tobacco hornworm, Manduca sexta (L.): growth of the last-instar larva and the decision to pupate. J. Exp. Biol. *61*, 481–491.

Nojima, S., Toyofuku, T., Kamao, H., Ishigami, C., Kaneko, J., Okuno, T., Takamatsu, H., Ito, D., Kang, S., Kimura, T., et al. (2013). A point mutation in Semaphorin 4A associates with defective endosomal sorting and causes retinal degeneration. Nat. Commun. *4*, 1406.

Ohhara, Y., Kobayashi, S., and Yamanaka, N. (2017). Nutrient-Dependent Endocycling in Steroidogenic Tissue Dictates Timing of Metamorphosis in Drosophila melanogaster. PLoS Genet. *13*, e1006583.

Ono, H., Rewitz, K.F., Shinoda, T., Itoyama, K., Petryk, A., Rybczynski, R., Jarcho, M., Warren, J.T., Marqués, G., Shimell, M.J., et al. (2006). Spook and Spookier code for stage-specific components of the ecdysone biosynthetic pathway in Diptera. Dev. Biol. *298*, 555–570.

Palm, W., and Thompson, C.B. (2017). Nutrient acquisition strategies of mammalian cells. Nature *546*, 234–242.

Palm, W., Sampaio, J.L., Brankatschk, M., Carvalho, M., Mahmoud, A., Shevchenko, A., and Eaton, S. (2012). Lipoproteins in Drosophila melanogaster—assembly, function, and influence on tissue lipid composition. PLoS Genet. *8*, e1002828.

Rajan, A., and Perrimon, N. (2012). Drosophila cytokine unpaired 2 regulates physiological homeostasis by remotely controlling insulin secretion. Cell *151*, 123–137.

Rees, J.S., Lowe, N., Armean, I.M., Roote, J., Johnson, G., Drummond, E., Spriggs, H., Ryder, E., Russell, S., St Johnston, D., and Lilley, K.S. (2011). In vivo analysis of proteomes and interactomes using Parallel Affinity Capture (iPAC) coupled to mass spectrometry. Mol. Cell. Proteomics *10*, M110, 002386.

Rewitz, K.F., Yamanaka, N., Gilbert, L.I., and O'Connor, M.B. (2009). The insect neuropeptide PTTH activates receptor tyrosine kinase torso to initiate metamorphosis. Science *326*, 1403–1405.

Rewitz, K.F., Yamanaka, N., and O'Connor, M.B. (2013). Developmental checkpoints and feedback circuits time insect maturation. Curr. Top. Dev. Biol. *103*, 1–33.

Romanauska, A., and Köhler, A. (2018). The Inner Nuclear Membrane Is a Metabolically Active Territory that Generates Nuclear Lipid Droplets. Cell *174*, 700–715.e18.

Schüpbach, T., and Wieschaus, E. (1989). Female sterile mutations on the second chromosome of Drosophila melanogaster. I. Maternal effect mutations. Genetics *121*, 101–117. https://doi.org/10.1093/genetics/121.1.101.

Summerville, J.B., Faust, J.F., Fan, E., Pendin, D., Daga, A., Formella, J., Stern, M., and McNew, J.A. (2016). The effects of ER morphology on synaptic structure and function in Drosophila melanogaster. J. Cell Sci. *129*, 1635–1648.

Swanson, J.A. (2008). Shaping cups into phagosomes and macropinosomes. Nat. Rev. Mol. Cell Biol. *9*, 639–649.

Thomas, A., Lee, P.J., Dalton, J.E., Nomie, K.J., Stoica, L., Costa-Mattioli, M., Chang, P., Nuzhdin, S., Arbeitman, M.N., and Dierick, H.A. (2012). A versatile method for cell-specific profiling of translated mRNAs in Drosophila. PLoS ONE *7*, e40276.

Thul, P.J., Åkesson, L., Wiking, M., Mahdessian, D., Geladaki, A., Ait Blal, H., Alm, T., Asplund, A., Björk, L., Breckels, L.M., et al. (2017). A subcellular map of the human proteome. Science *356*, eaal3321.

Tu, M.P., and Tatar, M. (2003). Juvenile diet restriction and the aging and reproduction of adult Drosophila melanogaster. Aging Cell *2*, 327–333.

van der Klaauw, A.A., Croizier, S., Mendes de Oliveira, E., Stadler, L.K.J., Park, S., Kong, Y., Banton, M.C., Tandon, P., Hendricks, A.E., Keogh, J.M., et al.; INTERVAL; UK10K Consortium (2019). Human Semaphorin 3 Variants Link Melanocortin Circuit Development and Energy Balance. Cell *176*, 729–742.e18.

Várnai, P., and Balla, T. (2006). Live cell imaging of phosphoinositide dynamics with fluorescent protein domains. Biochim. Biophys. Acta *1761*, 957–967.

Verstreken, P., Ohyama, T., Haueter, C., Habets, R.L., Lin, Y.Q., Swan, L.E., Ly, C.V., Venken, K.J., De Camilli, P., and Bellen, H.J. (2009). Tweek, an evolutionarily conserved protein, is required for synaptic vesicle recycling. Neuron *63*, 203–215.

Wang, J.L., Saha, T.T., Zhang, Y., Zhang, C., and Raikhel, A.S. (2017). Juvenile hormone and its receptor methoprene-tolerant promote ribosomal biogenesis and vitellogenesis in the *Aedes aegypti* mosquito. J. Biol. Chem. *292*, 10306–10315.

Welch, R.M. (1957). A Developmental Analysis of the Lethal Mutant L(2)gl of Drosophila Melanogaster Based on Cytophotometric Determination of Nuclear Desoxyribonucleic Acid (Dna) Content. Genetics *42*, 544–559.

Wishart, D.S., Jewison, T., Guo, A.C., Wilson, M., Knox, C., Liu, Y., Djoumbou, Y., Mandal, R., Aziat, F., Dong, E., et al. (2013). HMDB 3.0—The Human Metabolome Database in 2013. Nucleic Acids Res. *41*, D801–D807.

Woods, S.C., Seeley, R.J., Porte, D., Jr., and Schwartz, M.W. (1998). Signals that regulate food intake and energy homeostasis. Science *280*, 1378–1383.

Yamanaka, N., Rewitz, K.F., and O'Connor, M.B. (2013). Ecdysone control of developmental transitions: lessons from Drosophila research. Annu. Rev. Entomol. *58*, 497–516.

Yamanaka, N., Marqués, G., and O'Connor, M.B. (2015). Vesicle-Mediated Steroid Hormone Secretion in Drosophila melanogaster. Cell *163*, 907–919.

Yazdani, U., and Terman, J.R. (2006). The semaphorins. Genome Biol. *7*, 211.

Yu, H.H., Araj, H.H., Ralls, S.A., and Kolodkin, A.L. (1998). The transmembrane Semaphorin Sema I is required in Drosophila for embryonic motor and CNS axon guidance. Neuron *20*, 207–220.

Zinke, I., Kirchner, C., Chao, L.C., Tetzlaff, M.T., and Pankratz, M.J. (1999). Suppression of food intake and growth by amino acids in Drosophila: the role of pumpless, a fat body expressed gene with homology to vertebrate glycine cleavage system. Development *126*, 5275–5284.

## STAR★METHODS

### KEY RESOURCES TABLE

| REAGENT or RESOURCE | SOURCE | IDENTIFIER |
|---|---|---|
| **Antibodies** | | |
| mouse anti-Dlg | DSHB | Cat#4F3; RRID: AB_528203 |
| mouse anti-Fibrillarin | ThermoFisher Scientific | Cat#38F3; RRID: AB_2532241 |
| mouse anti-Lam Dm0 | DSHB | Cat#ADL84.12; RRID:AB_528338 |
| mouse anti-Wg | DSHB | Cat#4D4; RRID: AB_528512 |
| rabbit anti-Apolpp | Joaquin Culi, Kutty et al., 1996 | N/A |
| rabbit anti-GFP | Abcam | Cat#Ab290 |
| rabbit anti-IgG HRP-conjugated | Sigma-Aldrich | Cat# A9169 |
| rabbit anti-ILP2 | Hugo Stocker, Bader et al., 2013 | N/A |
| rabbit anti-Sema1a | Alex Kolodkin, Yu et al., 1998 | N/A |
| rat anti-*D*E-Cad | DSHB | Cat#DCAD2; RRID: AB_528120 |
| donkey anti-Mouse IgG (H+L) Highly Cross-Adsorbed Secondary Antibody, Alexa Fluor 555 | Invitrogen | Cat#A-31570; RRID: AB_2536180 |
| donkey anti-Mouse IgG (H+L) Highly Cross-Adsorbed Secondary Antibody, Alexa Fluor 647 | Invitrogen | Cat#A-31571; RRID: AB_162542 |
| donkey anti-Rabbit IgG (H+L) Highly Cross-Adsorbed Secondary Antibody, Alexa Fluor 555 | Invitrogen | Cat#A-31572; RRID: AB_162543 |
| donkey Anti-Rat IgG (H+L) Alexa Fluor® 647 AffiniPure | Jackson ImmunoResearch | Cat#712-605-153; RRID: AB_2340694 |
| **Chemicals, peptides, and recombinant proteins** | | |
| Vectashield mounting medium with DAPI | Vector Labs | Cat#H-1200 |
| DAPI-Fluoromount-G | Electron Microscopy Sciences | Cat#17984-24 |
| GIBCO Schneider's *Drosophila* Sterile Medium | Thermo Fisher | Cat#21720024 |
| Bromophenol blue | Sigma-Aldrich | Cat#B6131 |
| α-ecdysone | Sigma-Aldrich | Cat#9004 |
| 20-hydroxyecdysone | Sigma-Aldrich | Cat#H5142 |
| SuperScript III First-Strand Synthesis System for RT-PCR | Invitrogen | Cat#18080-051 |
| Power SYBR Green PCR Master Mix | Applied Biosystems | Cat#4367659 |
| Paraformaldehyde 16% solution | Electron Microscopy Sciences | Cat#15710 |
| Nile Red | Sigma-Aldrich | Cat#72485 |
| 1X cOmplete Mini EDTAfree protease inhibitor cocktail | Sigma-Aldrich | Cat#11836170001 |
| Phalloidin 633 | ThermoFisher | Cat#A22284 |
| **Critical commercial assays** | | |
| 20-Hydroxyecdysone enzyme immunoassay kit | Bertin Pharma | Cat#A05120 |
| Amplex Red Cholesterol Assay Kit | ThermoFisher Scientific | Cat#A12216 |
| BCA Protein Assay Kit | Pierce | Cat#23227 |
| Glucose (HK) Assay Kit | Sigma-Aldrich | Cat#GAHK20-1KT |
| RNeasy-Mini Kit | QIAGEN | Cat#74106 |
| RNase Free DNase Set | QIAGEN | Cat#79254 |
| **Experimental models: Organisms/strains** | | |
| *D. melanogaster: mir-8$^{NP5247}$-Gal4* | DGRC | 104917 |
| *D. melanogaster: NP2222-Gal4* | DRGC | 112830 |
| *D. melanogaster: phm$^{22}$-Gal4* | Kim Rewitz, Ono et al., 2006 | N/A |

(*Continued on next page*)

*Continued*

| REAGENT or RESOURCE | SOURCE | IDENTIFIER |
|---|---|---|
| *D. melanogaster: ppl-Gal4* | BDSC | 58768 |
| *D. melanogaster: twi, dmef2-Gal4* | Ana Carmena | N/A |
| *D. melanogaster: spok-Gal4.1.45* | BDSC | 80578 |
| *D. melanogaster: tub-Gal80$^{ts}$* | BDSC | 7019 |
| *D. melanogaster: EP-RpLP0-like* | BDSC | 27939 |
| *D. melanogaster: UAS-apolpp-HA* | Marko Brankatschk, Brankatschk and Eaton, 2010 | N/A |
| *D. melanogaster: UAS-GFP-RpL10Ab* | BDSC | 42681 |
| *D. melanogaster: UAS-H2B::YFP* | Bellaïche et al., 2001 | N/A |
| *D. melanogaster: UAS-Leptin* | Norbert Perrimon, Rajan and Perrimon, 2012 | N/A |
| *D. melanogaster: UAS-mCD8::GFP* | BDSC | 5137 |
| *D. melanogaster: UAS-PLCδ-PH-EGFP* | BDSC | 39693 |
| *D. melanogaster: UAS-Rab5.S43N* | BDSC | 42703 |
| *D. melanogaster: UAS-Rab5-YFP* | BDSC | 24616 |
| *D. melanogaster: UAS-Ras$^{V12}$* | BDSC, Karim and Rubin, 1998 | 64196 |
| *D. melanogaster: UAS-Rheb* | BDSC | 9688 |
| *D. melanogaster: UAS-RpL3.FLAG* | BDSC | 79223 |
| *D. melanogaster: UAS-RpS13.FLAG* | BDSC | 79222 |
| *D. melanogaster: UAS-S6K* | BDSC | 6910 |
| *D. melanogaster: UAS-S6K$^{TE}$* | BDSC | 6912 |
| *D. melanogaster: UAS-secGFP* | Marcos Gonzalez-Gaitan, Entchev et al., 2000 | N/A |
| *D. melanogaster: UAS-Sema1a$^{ECD}$* | BDSC | 65739 |
| *D. melanogaster: UAS-Sema1a$^{FL}$* | BDSC | 65734 |
| *D. melanogaster: UAS-Sema1a$^{IC}$* | BDSC | 65737 |
| *D. melanogaster: UAS-slif$^{UY681}$* | BDSC | 52655 |
| *D. melanogaster: UAS-Syt::GFP* | BDSC | 6925 |
| *D. melanogaster: 20XUAS-tdTomato-Sec61beta* | BDSC | 64747 |
| *D. melanogaster: UAS-upd2* | James Castelli, Hombría et al., 2005 | N/A |
| *D. melanogaster: UAS-upd2::GFP* | James Castelli, Hombría et al., 2005 | N/A |
| *D. melanogaster: UAS-VHH-GFP4::CD8::mCherry* | Markus Affolter, Harmansa et al., 2015 | N/A |
| *D. melanogaster: UAS-Ilp8$^{i}$* | VDRC | v102604 |
| *D. melanogaster: UAS-Pten$^{i}$* | VDRC | v101745 |
| *D. melanogaster: UAS-RpL10Ab$^{i}$* | BDSC | 34695 |
| *D. melanogaster: UAS-RpS3$^{i}$* | BDSC | 31625 |
| *D. melanogaster: UAS-RpS6$^{i}$* | BDSC | 32418 |
| *D. melanogaster: UAS-RpS13$^{i}$* | BDSC | 34820 |
| *D. melanogaster: UAS-TOR$^{i}$* | BDSC | 33951 |
| *D. melanogaster: UAS-TOR$^{i}$* | BDSC | 34639 |
| *D. melanogaster: Sema1a$^{P2}$* | Liqun Luo, Yu et al., 1998 | N/A |
| *D. melanogaster: Sema1a$^{MI00031\text{-}GFSTF.2}$* | BDSC | 60140 |
| *D. melanogaster: upd2$^{\Delta 3\text{-}62}$* | James Castelli, Hombría et al., 2005 | N/A |
| *D. melanogaster: tor$^{RL3}$* | Jordi Casanova, Schüpbach and Wieschaus, 1989 | N/A |
| *D. melanogaster: w1118* | Morante lab | N/A |
| Deposited data | | |
| $^{1}$H NMR | This study | https://doi.org/10.5281/zenodo.5520983 |
| WB | This study | https://doi.org/10.17632/t946n47rtk.1 |

(*Continued on next page*)

*Continued*

| REAGENT or RESOURCE | SOURCE | IDENTIFIER |
|---|---|---|
| Oligonucleotides | | |
| RT-qPCR primers | This study | See Table S6 |
| Software and algorithms | | |
| ZEN blue 2.3 | Zeiss | N/A |
| ImageJ/Fiji | NIH | N/A |
| Prism8 | GraphPad Software | N/A |
| Photoshop CS5 | Adobe | N/A |
| Illustrator CS5 | Adobe | N/A |
| Microsoft Word 2016 | Microsoft Corporatsion | N/A |
| Microsoft Excel 2016 | Microsoft Corporation | N/A |
| Cytoscape 3.8.0 | Cytoscape Consortium | N/A |
| Other | | |
| Zeiss LSM 880 confocal microscope with Airyscan | Zeiss | N/A |
| Leica TCS SP2 confocal microscope | Leica | N/A |
| ABI7500 apparatus | Applied Biosystems | N/A |
| Bruker Ultrashield Plus 600 MHz spectrometer | Bruker Corporation | N/A |
| Infinite M200 Pro Microplate Reader | Tecan | N/A |

## RESOURCE AVAILABILITY

### Lead contact

Further information and requests for resources and reagents should be directed to and will be fulfilled by the lead contact, Javier Morante (j.morante@umh.es).

### Materials availability

This study did not generate new unique reagents

### Data and code availability

- Original western blot image has been deposited at Mendeley and is publicly available as of the date of publication. Integration peaks of $^{1}$H nuclear magnetic resonance spectroscopy (NMR) data have been deposited at Zenodo. Both DOIs are listed in the Key resources table. Super-resolution microscopy data reported in this paper will be shared by the lead contact upon request.
- This paper does not report original code.
- Any additional information required to reanalyze the data reported in this paper is available from the lead contact upon request.

## EXPERIMENTAL MODEL AND SUBJECT DETAILS

### *Drosophila* Husbandry

Fly stocks used in this study were: mir-8$^{NP5247}$-Gal4 (DGRC #104917), NP2222-Gal4 (DGRC #112830), phm$^{22}$-Gal4 (a gift from K. Rewitz), ppl-Gal4 (BDSC #58768), twi, dmef2-Gal4 (a gift from A. Carmena), spok-Gal4.1.45 (BDSC #80578), tub-Gal80$^{ts}$ (BDSC #7019), EP-RpLP0-like (BDSC #27939), UAS-apolpp-HA (Brankatschk and Eaton, 2010; a gift from M. Brankatschk), UAS-GFP-RpL10Ab (BDSC #42681), UAS-H2B::YFP (Bellaïche et al., 2001), UAS-Leptin (Rajan and Perrimon, 2012; a gift from N. Perrimon), UAS-mCD8::GFP (BDSC #5137), UAS-PLCδ-PH-EGFP (BDSC #39693), UAS-Rab5.S43N (BDSC #42703, also called Rab5$^{DN}$), UAS-Rab5-YFP (BDSC #24616), UAS-Ras$^{V12}$ (BDSC #64196), UAS-Rheb (BDSC #9688), UAS-RpL3.FLAG (BDSC #79223, Chen and Dickman, 2017), UAS-RpS13.FLAG (BDSC #79222; Chen and Dickman, 2017), UAS-S6K (BDSC #6910), UAS-S6K$^{TE}$ (BDSC #6912), UAS-secGFP (Entchev et al., 2000; a gift from M. Gonzalez-Gaitan), UAS-Sema1a$^{ECD}$ (BDSC #65739), UAS-Sema1a$^{FL}$ (BDSC #65734), UAS-Sema1a$^{IC}$ (BDSC #65737), UAS-slif$^{UY681}$ (BDSC #52655, also called slif$^{ANTI}$), UAS-Syt::GFP (a gift from B. Hassan), UAS-tdTomato-Sec61β (BDSC #64747, (Summerville et al., 2016), UAS-upd2 (Hombría et al., 2005, a gift from J. Castelli), UAS-upd2::GFP (Hombría et al., 2005, a gift from J. Castelli), UAS-VHH-GFP4::CD8::mCherry (Harmansa et al., 2015, a gift from M. Affolter), UAS-Ilp8$^{i}$ (VDRC, kk112161, v102604), UAS-Pten$^{i}$ (VDRC, kk109278, v101745), UAS-RpL10Ab$^{i}$ (HMS01174, BDSC #34695), UAS-RpS3$^{i}$ (JF01410, BDSC #31625), UAS-RpS6$^{i}$ (HMS00413, BDSC #32418), UAS-RpS13$^{i}$ (HMS00135, BDSC

#34820), UAS-TOR$^{i}$ RNAi#1 (HMS00904, BDSC #33951), UAS-TOR$^{i}$ RNAi#2 (HMS01114, BDSC #34639), Sema1a$^{P2}$ (Yu et al., 1998, a gift from L. Luo), Sema1a$^{MI00031\text{-}GFSTF.2}$ (BDSC #60140), upd2$^{\Delta 3\text{-}62}$ (Hombría et al., 2005, a gift from J. Castelli), tor$^{RL3}$ (Schüpbach and Wieschaus, 1989, a gift from J. Casanova) and w$^{1118}$.

Flies were reared in standard "Iberian" fly food at 25°C on a 14:10 h light:dark cycle (surrogate of laboratory summer time). Standard "Iberian" fly food was made by mixing 15 L of water, 0.75 kg of wheat flour, 1 kg of brown sugar, 0.5 kg yeast, 0.17 kg agar, 130 mL of a 5% nipagin solution in ethanol, and 130 mL of propionic acid.

### Screenings of Nutrient Transporters, Secreted and Transmembrane Factors by RNA$^{i}$

The lists of *RNA$^{i}$* transgenes (Dietzl et al., 2007; Ni et al., 2011) used are in Tables S1 and S2 (in red, lines producing phenotype).

## METHOD DETAILS

### Measurement of the Developmental Timing of Pupation

We crossed 20–30 females and 20–30 males. After 24–48 hours, flies were transferred to grape juice agar plates with yeast paste and left for 4 hours to allow egg deposition. Parental flies were removed, and laid eggs were incubated for 48 hours at 25°C. Second-instar larvae were transferred onto 5 mL of *Drosophila* standard "Iberian" food (20 larvae per tube) and reared at 25°C. A survey of the pupae was performed at 8-hour intervals; 2-4 hours after initiation of egg laying was considered time "0" and referred to as "after egg laying (AEL)." For the developmental time-course analysis of ring glands using super-resolution imaging, survey of L2/L3 molting timing was used for carefully stage of the gland ($n \geq 15$ gland per time point).

### Immunohistochemistry in Larval Imaginal Discs, Fat bodies and Brains

Control (at 112 hours AEL) and mutant (at 112 and 256 hours AEL) larval brains, fat bodies and imaginal discs were dissected out in cold Phosphate-buffered saline (PBS) buffer and fixed in 4% paraformaldehyde for 20 minutes (Morante and Desplan, 2011). Brains, fat bodies and imaginal discs were stained overnight at room temperature with the following primary antibodies: mouse anti-Dlg 4F3 (1/100, DSHB), mouse anti-fibrillarin 38F3 (1/500, ThermoFisher), mouse anti-Lam Dm0 ADL84.12 (1/200, DSHB), mouse anti-Wg 4D4 (1/100, DSHB), rabbit anti-Apolpp (1/500 (Kutty et al., 1996), a gift from J. Culi), rabbit anti-ILP2 (1/500; Bader et al., 2013), rabbit anti-Sema1a (1/5000 (Yu et al., 1998), a gift from A. Kolodkin), and rat anti-*D*E-Cad DCAD2 (1/50, DSHB). Secondary antibodies were purchased from Invitrogen and Jackson ImmunoResearch. Fat bodies in Figure S4 were also incubated for 1 hour at 1:40 dilution of PBS with Phalloidin 633 (ThermoFisher, A22284) at room temperature.

### Super-resolution Confocal Imaging of Larval Brains, Fat Bodies and Prothoracic Gland Cells

Larval brains and fat bodies were mounted in Vectashield mounting medium with DAPI (H-1200, Vector Labs), maintaining their 3D configuration (Morante and Desplan, 2011). Imaginal discs were mounted with DAPI-Fluoromount-G (17984-24, Electron Microscopy Sciences). Images were obtained on a Leica TCS SP2 confocal microscope and a Zeiss LSM 880 confocal microscope with Airyscan, a module for super-resolution based on an array detector with laser scanning confocal microscopy.

### Neutral Lipid Staining and Quantification in Larval Brains

To label neutral lipids, after incubating with corresponding secondary antibodies, larval brains were rinsed three times with PBS, and then incubated for 40 min at 1:500 dilution of PBS with 1 mg/ml Nile Red (Sigma-Aldrich). Image acquisition used identical laser power and scan settings for any conditions and time points. ImageJ software was used to measure total fluorescent intensity at 555 nm across larval brains.

### Bromophenol Blue Incorporation

Bromophenol blue (3′,3″,5′,5″-tetrabromophenolsulfonphthalein) was dissolved in standard "Iberian" fly food. Control feeding (*phm* > + at 48 h AEL) and mutant larvae (*phm* > *Sema1a$^{i}$* at 240 h AEL) were transferred to fly food with bromophenol blue and incubated for 24 hours.

### α-Ecdysone and 20-Hydroxyecdysone (20E) Treatments

Second-instar larvae (48 h AEL) were collected as described above and transferred to fresh Iberian food. Control (*phm* > +) and mutant larvae (*phm* > *Sema1a$^{i}$*) were transferred to fresh food with 0.5 mg/mL of α-ecdysone (E9004, Sigma-Aldrich) or 20-hydroxyecdysone (H5142, Sigma-Aldrich) diluted in ethanol at 72 hours and 256 hours AEL. We used ethanol as a control (vehicle for α-ecdysone and 20-hydroxyecdysone).

### Hemolymph Sample Preparation

Larvae were rinsed in PBS and dried in tissue paper. Then they were individually immersed in Schneider's medium and their cuticles carefully torn to release the hemolymph. Total hemolymph of 15 larvae (three replicates from control and mutant animals) was stored at −80°C until use in 1 × Reaction Buffer (total volume, 50 μl). Fifty μL of these samples were subjected to cholesterol quantification.

### Ecdysteroid Measurements

Whole-larvae from 20 control (*phm* > ) or mutant (*phm* > *Sema1a*$^{i}$ and *phm* > *upd2*$^{i}$) from 96 hours and 120 hours AEL were collected and preserved as described in Koyama and Mirth (2021). 20E titers were measured by ELISA in duplicate following the instructions of a commercially-available 20-Hydroxyecdysone enzyme immunoassay kit (Bertin Pharma #A05120.96 wells). Absorbance was measured at 410 nm on an Infinite M200 Pro Microplate Reader (Tecan, Männedorf, Switzerland) using Software i-control 1.6.

### Metabolomic Footprinting

Metabolites were quantified using proton nuclear magnetic resonance (NMR) spectroscopy. Twenty frozen larvae (−80°C) (six replicates) were placed on ice and allowed to thaw for 5 min. 240 μL of methanol, 48 μL of deionized water and 200 μL of chloroform were added at 4°C. After 10 min, samples were homogenized with a small plastic pestle for 2 min and resuspended with a pipette. For uniform cell breakage, the samples were placed in liquid nitrogen for 1 min and then allowed to thaw on ice for 2 min. This step was repeated twice more. Afterward, 120 μL of deionized water and 120 μL of chloroform at 4°C were added, and the samples vortexed. Then the samples were centrifuged at 10,000 g for 15 min at 4°C to allow phase separation into an aqueous (top) and an organic phase (bottom), containing polar and non-polar compounds, respectively. Each phase was transferred to different tubes, and the remaining solvent from the other phase discarded. The aqueous phase was lyophilized overnight to remove water and methanol. Nitrogen gas was used to remove the chloroform of the organic phase. Extracts were stored at −80°C until NMR sample preparation and measurement.

For NMR analysis, samples were placed on ice and allowed to thaw for 5 min. Then 550 μl of phosphate buffer (100 mM $Na_2HPO_4$ pH 7.4, in 100% $D_2O$) containing 0.1 mM 3-(trimethylsilyl) propionic-2,2,3,3-d4 acid sodium salt (TSP), as internal standard, was added to the aqueous phase. The samples were resuspended and the supernatants transferred into a 5-mm NMR tube. The organic phase was dissolved in 600 μl of deuterated chloroform ($CDCl_3$) with 0.0027% tetramethylsilane (TMS) as the internal standard. Samples were vortexed, transferred into a 5 mm NMR tube and the tube sealed.

Samples were analyzed on a Bruker Ultrashield Plus 600 MHz spectrometer equipped with a 5 mm TCI Cryoprobe. For aqueous samples, a 1D NOESY pulse sequence with water pre-saturation and gradients, with a 12016 Hz spectral width, 65536 data points, acquisition time of 2.7 s, relaxation delay of 4 s and 400 scans was acquired at 27°C. For organic samples, a standard $^{1}$D $^{1}$H pulse sequence, with a 12016 Hz spectral width, 65536 data points, acquisition time of 2.7 s, relaxation delay of 4 s and 128 scans was acquired. Spectra were processed with exponential line broadening to 0.5 Hz and zero filling to 128000 points was acquired at 25°C. Total correlation spectroscopy (TOCSY) and multiplicity heteronuclear single quantum correlation (HSQC) were performed for representative samples of the aqueous phase and the organic phase from both sample types for signal assignment. For each of these experiments, 256–512 $t_1$ increments were used and 32–96 transients were collected. The relaxation delays were set to 1.5 s and the experiments were acquired in the phase-sensitive mode. TOCSY spectra were recorded using a standard MLEV-17 pulse sequence with mixing times (spin-lock) of 65 ms.

Following Fourier transformation, 1D spectra were manually phased, baseline-corrected and referenced to the TSP peak (aqueous phase, 0.00 ppm) or the TMS peak (organic phase, 0 ppm) using MestReNova 8.1. Metabolite identities were assigned by comparison to reference values for chemical shift and multiplicity, and confirmed by comparison to spectra of pure compounds in the Human Metabolome database (Wishart et al., 2013).

Integration tables and lipid level data (Tables S4 and S5) were normalized to total intensity of the NMR spectra, which represents the total amount of aqueous or lipidic metabolites, respectively, scaled to unit variance and mean centered. For quantitative comparison, metabolite signals were integrated with MestReNova 8.1 using the GSD deconvolution option. The integration tables for the metabolomics data were deposited at Zenodo repository (https://doi.org/10.5281/zenodo.5137738).

### Quantitative RT-PCR

To assess mRNA levels, total RNA was extracted from five *Drosophila* larvae using the RNeasy-Mini Kit (QIAGEN). To remove contaminating DNA, RNA was treated with RNase Free DNase Set (QIAGEN). cDNA was synthesized with the SuperScript III First-Strand Synthesis System for RT-PCR (Invitrogen) using random oligo-dT primers (Invitrogen). Quantitative real time PCR was performed using SYBR Green PCR Master Mix (Applied Biosystems) with gene-specific primers, on an ABI7500 apparatus (Applied Biosystems). Normalization was done using the ribosomal gene *RP49* and/or *β-actin* (Figure S5A). Comparative qPCRs were performed in triplicate and the relative expression was calculated using the comparative Ct method. The primer sequences used for this study are given in Table S6.

### Western Blot

For western blot, hemolymph samples were collected from 20 larvae in a protease inhibitor solution (1X cOmplete Mini EDTAfree protease inhibitor cocktail (Sigma-Aldrich)) diluted in PBS). Protein concentration of samples were determined using BCA Protein Assay Kit (Pierce). 20 μg of protein was separated for each sample on a 4%–12% SDS-PAGE gel and transferred to a PVDF membrane (InmovilonP Transfer membranes, Millipore). Blot membrane was incubated in Ponceau S staining solution for 3 minutes at room temperature and then rinsed with distilled water. An image of this staining was taken as loading control.

Blot membrane was blocked (0.1% Tween20 in PBS supplemented with 3% BSA) for 1 hour at room temperature, and then incubated overnight at 4°C with a rabbit antibody against GFP (Abcam Ab290) in a 1:1000 dilution (in 0.1% Tween20 in PBS

supplemented with 3% BSA). Next day, membrane was incubated in HRP-conjugated rabbit a-IgG (Sigma-Aldrich) in a 1:20.000 dilution (in 0.1% Tween20 in PBS supplemented with 3% BSA). Protein was detected using the chemiluminescent substrate ECL (Pierce).

## QUANTIFICATION AND STATISTICAL ANALYSIS

### Measurements of GFP, ILP2, Apolpp Content, and Imaginal Disc and Vesicle Size

Fluorescence intensity measurements were performed using ImageJ analyses of cytoplasmic GFP or Apolpp staining in the corresponding tissues from carefully staged larvae reared at 25°C ($n \geq 100$ ROI (Regions of interest) and > 5 larvae per genotype or condition or time-point). Plot in Figure 5M represents integrated density (area × mean ROI pixel intensity) between control and obese mutant larvae.

Larval imaginal wing disc areas were measured using ImageJ.

### Cholesterol Quantification

Cholesterol levels in wandering control (*phm* > at 112 h AEL) and mutant larval (*phm* > *Sema1a*$^{i}$ at 112 h and 256 h AEL) brains, fat bodies and hemolymphs (three replicates of 15 animals per group) were determined using the Amplex Red Cholesterol Assay Kit (ThermoFisher Scientific) according to the manufacturer's directions.

### Glucose Measurement

Glucose levels in wandering control (*phm* > at 112 h AEL) and mutant larval (*phm* > *Sema1a*$^{i}$ at 112 h and 256 h AEL) hemolymphs (three replicates of 15 animals per group) were determined using the GAHK20 Glucose Assay kit (Sigma-Aldrich), according to the manufacturer's directions.

### Weight and Size Measurements

For weighing larval flies, 30-45 larvae of each genotype were collected at required developmental stages and weighed using a precision scale.

For larval and pupal volume determination, 10 larvae and pupae of each genotype were collected and photographed with their dorsal side up, and length and width were measured using ImageJ. Volume was calculated according to the following formula $v = (4/3)\ \pi(L/2)^{*}(w/2)^{2}$ (L, length; w, width).

### DNA Quantification and Nuclear Size of PG Cells

To measure DNA density in PG and nuclear area of the cells, super-resolution z stacked images of DAPI-stained PG glands were obtained. The reference diploid (2n) was the DNA staining intensity value in brain lobe cells. The intensity of DNA staining in PG was divided by the intensity in the brain lobe. Quantifications were performed per nuclei (individual ROI). After 2n background subtraction, the C value of the control PG cells at 112 h AEL was normalized at 64C according to (Ohhara et al., 2017; Welch, 1957). ImageJ software was used to quantify the intensity of DAPI.

### Statistical Analysis

All statistical analyses were performed using GraphPad Software 8.0 with a 95% confidence limit ($p < 0.05$). The experimental data are presented as means ± SEM using a one-way or two-way analysis of variance (ANOVA) followed by Bonferroni's post hoc test for comparing more than two genotypes and time-points. An unpaired t test was used for comparisons between two genotypes or time-points.